MAXIMUM WEIGHT LIFTING PREDICTION CONSIDERING DYNAMIC JOINT STRENGTH

By

G M Rahid uz zaman Rana, B.S.

A Thesis Submitted in Partial Fulfillment of the Requirements

For the Degree of

Master of Science

In

Mechanical Engineering

University of Alaska Fairbanks

May 2018

APPROVED:

Dr. Yujiang Xiang, Committee Chair
Dr. Cheng-fu Chen, Committee Member
Dr. Rorik Peterson, Committee member
Dr. Rorik Peterson, Chair
Department of Mechanical Engineering
Dr. Doug Goering, Dean
College of Engineering and Mines
Dr. Michael Castellini, *Dean of Graduate School*

Abstract

This thesis describes an efficient optimization method for predicting the maximum lifting weight considering dynamic joint strength in symmetric box lifting using a skeletal model. Dynamic joint strength is modeled as a three-dimensional function of joint angle and joint angular velocity based on experimentally obtained joint strength data. The function is further formulated as the joint torque limit constraint in an inverse dynamics optimization formulation to predict the lifting motion. In the proposed optimization formulation, external load is treated as design variables along with joint angle profiles, which are represented by control points of B-spline curves. By using this new formulation, dynamic lifting motion and strategy can be predicted for a symmetric maximum weight box lifting task with given initial and final box locations. Results show that incorporating dynamic strength is critical in predicting the lifting motion in extreme lifting conditions. The prediction outputs in joint space are incorporated in OpenSim software to find out muscles force and activity during the movement. Electromyography data are collected for a regular weight lifting to validate the integration process between the predictive model (joint model) and OpenSim model (muscle model). The proposed algorithm and analysis method based on motion prediction and OpenSim can be further developed as a useful ergonomic tool to protect workers from injury in manual material handling.

Table of Contents

List of Figures

List of Tables

Chapter 1 Introduction

1.1 Motivation and Objectives

Manual material handling, particularly lifting, poses a risk to many workers and is considered a major cause of work-related low back pain and impairment. The National Institute of Occupational Safety and Health (NIOSH) lifting equation is a well-known tool for injury prediction in box lifting. However, the NIOSH lifting equation only considers static lifting conditions and thus is not accurate for a specific subject's dynamic motion generation and injury control. Lifting is a dynamic activity, and therefore joint torque and forces must be calculated through dynamic calculations, not merely static ones.

The primary objective of this study is to predict maximum weight during lifting for a human skeletal model considering dynamic joint strength and analyze the muscles for that particular motion in OpenSim (muscle model) to find out risky or heavily loaded muscles. EMG data are used to validate this integration process. The ultimate goal is to develop a subject-specific ergonomic tool to protect workers from injury for symmetric lifting tasks.

1.2 Background

1.2.1 Lifting Simulation

For the last few decades, researchers have mainly used three methods to analyze lifting: the physiological approach, psychophysical approach, and biomechanical approach. The physiological approach is related to human metabolism, heart rate, oxygen consumption, intake energy, and energy expenditure. Using this methodology, safe and tolerable work periods have

been determined. Mathematical models exist to predict motion and maximum lifting weight based on oxygen uptake ((Aberg, Elgstrand, Magnus, & Lindholm, 1967; Asfour, 1980; Frederik, 1959) or energy cost (Asfour, 1980) in the case of manual lifting.

The psychophysical approach, a branch of psychology, is based on human feeling, physical stimuli, and sensory response. The maximum lifting weight is related to the following psychophysical factors: (1) excessive fatigue or discomfort (Switzer, 1962), (2) width of the box (McConville, 1992), (3) speed of work (V. Ciriello, S. Snook, A. Buck, & P. Wilkinson, 1990; Snook & Ciriello, 1974), (4) frequency of work (Knipfer, 1974; A. Pinder & M. Boocock, 2014; Pinder, 1997), and (5) a combination of lifting heights, frequency, and box size (M. Ayoub & Dempsey, 1999; M. M. Ayoub, 1989). Some psychophysical models that predict the maximum lifting weight consider the effect of lifting height, use of bag instead of box, or task and operator variables (M. M. Ayoub, 1989; Osgood, 1980; Pytel & Kamon, 1981).

For all the above-mentioned approaches, however, it is difficult to predict human motion. Researchers had to use human subjects for every experiment, and it is risky to use human subjects to determine the maximum weight-lifting motion.

Compared with the experimental method of using human subjects to assess problems during lifting, biomechanical models can provide relatively new alternative technologies that allow direct testing and subject-specific results. In general, there are two major categories of lifting prediction using biomechanical models: optimization-based approaches and index-based approaches. Optimization-based approaches are further divided into static posture prediction for lifting (Dysart & Woldstad, 1996; Kothiyał, Mazumdar, & Noone, 1992; Noone & Mazumdar, 1992) and dynamic lifting motion prediction (Arisumi, Chardonnet, Kheddar, & Yokoi, 2007; M. Ayoub, 1992; Huang, Sheth, & Granata, 2005; Lee, 1988; Song, Qu, & Chen, 2016; Yujiang

Xiang, Jasbir S Arora, & Karim Abdel-Malek, 2012; Xiang, Arora, Rahmatalla, et al., 2010). In the index-based approaches, the lifting strategy was quantified by defining certain indexes (Burgess-Limerick & Abernethy, 1997a; Freivalds, Chaffin, Garg, & Lee, 1984; Zhang, Nussbaum, & Chaffin, 2000). For example, Burgess-Limerick and Abernethy (Burgess-Limerick & Abernethy, 1997b) used the index as the ratio of knee flexion to the sum of ankle, hip, and lumbar spine flexion to quantify the static starting posture. The relatively large value index was for squat lifting; a small value was for stoop lifting.

Many strategies could be chosen to suit the lifting task, depending on anthropometry, lifting weight, and object position and shape. Dynamic motion optimization has a better chance of predicting the different strategies. Lifting motion prediction is essentially an optimal control problem. The motion is generated using certain optimization principles with given boundary conditions. The direct optimization method transfers the optimal control problem into a nonlinear programming (NLP) problem (Xiang, Arora, & Abdel-Malek, 2010). The NLP formulation has three basic elements, the design variables, an objective function, and constraints. A key element in NLP formulation is the equations of motion (EOM), which impose the law of physics for the biomechanical system. There are three basic ways to incorporate the EOM in the optimization formulation: forward dynamics optimization (Shourijeh & McPhee, 2014; Darryl G Thelen & Frank C Anderson, 2006), inverse dynamics optimization (Farahani, Andersen, de Zee, & Rasmussen, 2016; Fregly, Reinbolt, Rooney, Mitchell, & Chmielewski, 2007; Ren, Jones, & Howard, 2007; Xiang, Arora, Rahmatalla, & Abdel-Malek, 2009; Xiang, Arora, Rahmatalla, et al., 2010), and optimization with direct collocation (Ackermann & Van den Bogert, 2010; Arora & Wang, 2005). The latter two formulations are computationally efficient because numerical integration is not required during the optimization process. However, forward dynamics

optimization gives more accurate mechanical system response because the numerical integration requires a much smaller time step length compared with the time grid points where the EOM and constraints are evaluated during the optimization process.

Although researchers are diligently exploring different types of cost functions for human motion predictions, constraints are also critical in predicting accurate human motions. Some physical constraints, such as joint angle limits and joint torque limits, must be enforced throughout the motion. For joint torque limits, there are static strength (constant torque limit) and dynamic strength (torque limit as a function of time). Many simulations reported in the literature used static strength for approximation (Ackermann & Van den Bogert, 2010; Davoudabadi Farahani, Andersen, de Zee, & Rasmussen, 2015; Fregly et al., 2007; Ren et al., 2007; Song et al., 2016; Xiang, Arora, Rahmatalla, & Abdel-Malek, 2009; Xiang, Arora, Rahmatalla, et al., 2010). Dynamic joint strength has been experimentally tested and reported in the literature (Cahalan, Johnson, Liu, & Chao, 1989; Frey-Law et al., 2012; Sara J Hussain & Laura Frey-Law, 2016; Kumar, 1996; Looft, 2014), but only a few have been used in simulation to predict more accurate human motion, such as reported in Farizeh and Sadigh (Farizeh & Sadigh, 2017) who studied a fast-walking problem. The literature shows that lifting frequency (kg/min), particularly a higher frequency, has an impact on joint strength as well as on prediction of maximum acceptable weights (V. M. Ciriello, S. H. Snook, A. C. Buck, & P. L. Wilkinson, 1990; Pinder, 1997; A. D. J. Pinder & M. G. Boocock, 2014). Therefore, it is important to use dynamic strength instead of static strength for motion prediction under extreme conditions.

1.2.2 Muscle modelling

Muscle is a complex part of human body and modelling it relates to a lot of parameters like muscle forces, muscle lengths, tendon strains, neural excitations and activations etc. It is extremely

difficult to measure these neuromuscular quantities for many muscles which are related to various movements. Since biological muscles are very complex, a lot of assumptions and simplifications are made for developing the mathematical model of muscle, such as Zajac (Zajac, 1989) assumed that muscle fibers are of equal, straight, parallel and coplanar. There are mainly two types of muscle model: one is cross bridge model (Eisenberg, Hill, & Chen, 1980; Haselgrove & Huxley, 1973; Zahalak & Ma, 1990) and another one is Hill-type model (Marcelo Epstein 1998; Winters & Stark, 1987; Zajac, 1989). Cross bridge models are not considered for many muscles and a lot of parameters are difficult to measure. Hill type models are extensively used to simulate muscle driven simulations (Anderson & Pandy, 2001; Arnold & Delp, 2011; Selbie & Caldwell, 1996; Van der Krogt, Delp, & Schwartz, 2012; Zajac, Neptune, & Kautz, 2002, 2003). The software OpenSim is extensively used in Biomechanics field to analyse muscle activities. This software is based on the Thelen muscle model (Thelen, 2003; D. G. Thelen & F. C. Anderson, 2006) and Millard muscle model (M. Millard, T. Uchida, A. Seth, & S. L. Delp, 2013) which are also Hill type muscle models.

Muscle consist of a lot of fasciculus (or fascicle) which are actually a bundle of skeletal muscle fibers surrounded by connective tissues. The inner layer of muscle belly and outer layer of fascicle is called epimysium. Every fascicle consists of fibers. The inner layer of fascicles and outer layer of fibers are called endomysium. Fibers consists of myofibril at microscopic level (Figure 1.1)

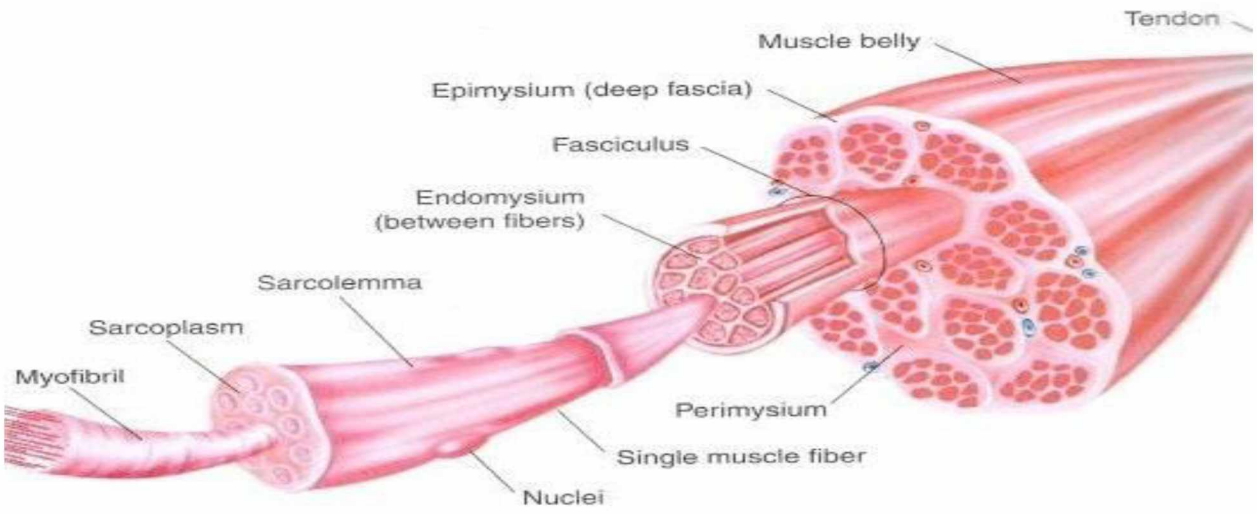

Figure 1. 1 Muscle Physiology (Stovall, 2013)

Inside Sarcomere there are Z-bands which are consists of actin and myosin (Figure 1.2). When actin and myosin react with each other, myosin contracts. Normally, they cannot react with each other because there is a protein layer on actin called troponin which resists actin to react with myosin. Also, the ends of myosin are connected with Z-band of sarcomere. When central nervous system (CNS) sends signal to activate a muscle, the Ca^{+} concentration increases nearby the muscles actin and myosin. Then Troponin reacts with Ca^{+}. As a result, myosin gets some space to react with actin and contracts. When myosin tries to contract, it ultimately pulls both side of Z-bands as well as sarcomere inward. Because of this contraction in every sarcomere of a muscle the whole muscle contracts and moves a particular segment of body.

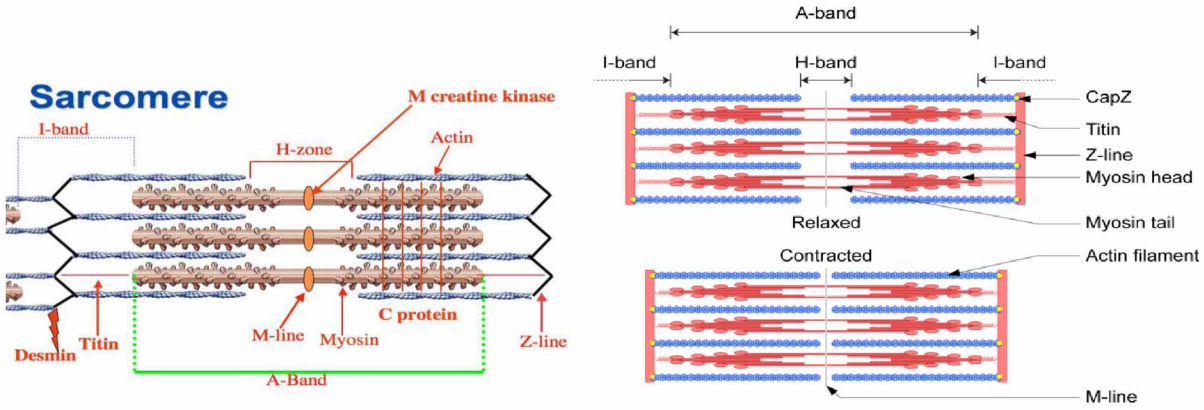

Figure 1. 2 Ratcheting mechanism of actin and myosin (Delsys, 2018; Willms, 2012)

Based on muscle physiology, Hill gave a muscle model which consists of three parts as shown in Figure 1.3. First, contractile elements represent the energy output from the ratcheting mechanism of actin and myosin. The tendon and connective tissues are represented by two elastic elements. One is series elastic elements (SEE) and another one is passive or parallel elastic elements.

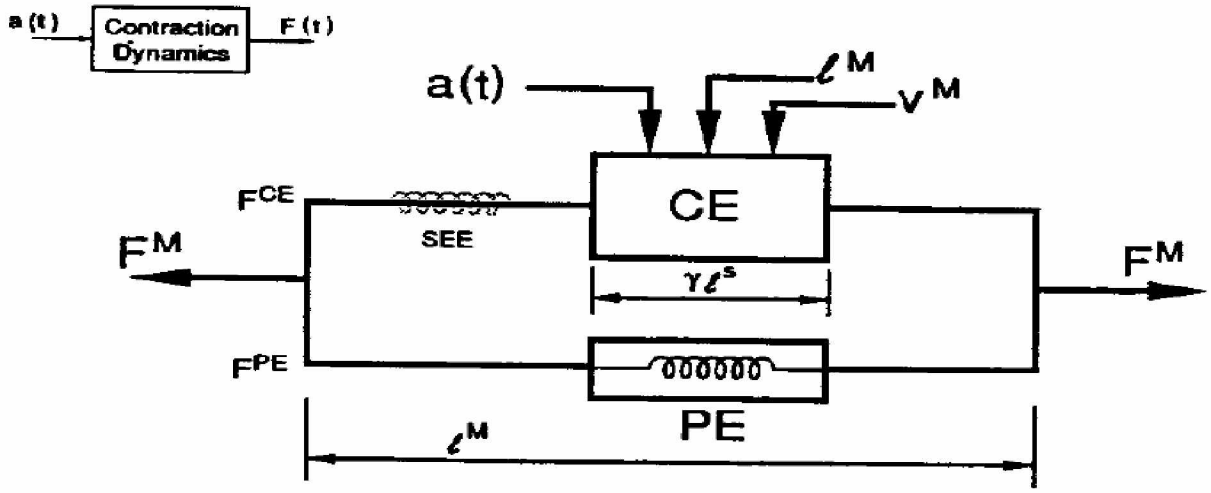

Figure 1. 3 Hill muscle model (Hill, 1949)

1.3 Overview of thesis and specific contribution

This thesis is organized as follows: In Chapter 2, a 2D skeletal model that has 10 degrees of freedom is built based on DH method. Coordinate systems and equations of motion are expressed in this chapter. The constraints for optimization are discussed in Chapter 3. New optimization formulation is proposed considering external force and time grid as design variables. Also, the dynamic joint strengths are considered as constraints which help us to predict maximum lifting weight.

In Chapter 4, the simulation results for maximum weight lifting are discussed.

In Chapter 5, the predictive model results in joint space will be inserted in OpenSim software to find out risky or heavily loaded muscles for that particular motion.

In Chapter 6, we collect electromyography (EMG) data from muscles to validate the integration process between the prediction model and OpenSim muscle model in chapter 5.

Finally, the thesis ends with chapter 7 having conclusions and plan of future research.

The research contributions of this work are summarized as follows:

(1) A new methodology had been developed to predict the maximum lifting weight and motion by considering dynamic joint strength for symmetric lifting tasks using a skeletal model. The simulation CPU time was close to real time.

(2) The proposed dynamic optimization method was able to predict novel dynamic lifting strategies for maximum weight lifting based on given inputs such as box location and subject's strength. The maximum weight lifting can activate major joint dynamic strength. This depends on the predicted lifting strategy for the given task.

(3) Based on the prediction, muscle model was analyzed in OpenSim for lifting motion to find out risky or heavily loaded muscles for extreme loading condition.

(4) To validate this integration, electromyography (EMG) data were collected and analyzed for those muscles.

Chapter 2 Human Modelling, Kinematics, and Dynamics

Two-dimensional (2D) models of the human body are widely used in biomechanics to simulate and analyze human movement because of computational simplicity. As left and right side joints angles are considered symmetric in 2D models, only symmetric motion can be simulated. A 2D skeletal model with ten degrees of freedom (DOF) defined in the joint space is used to simulate a symmetric lifting motion as shown in Figure 2.1. Among the ten DOF, three DOF are used for global translation (GT1 and GT2) and global rotation (GR1) and seven (Q4 to Q10)) for the body joints. The global DOF are composed of two translational (prismatic) joints and one rotational (revolute) joint. The anthropometric data for the skeletal model representing a 50th percentile male are generated using GEBOD® software. Link lengths, masses and moments of inertia are shown in Table 2.1.

Table 2. 1 Link length, mass, and moment of inertia

Link name	Link length (m)	Link mass (kg)	Moment of inertia, I_{ZZ} ($kg \cdot m^2$)
Link 1 (L1)	0.435	20.84	0.8933
Link 2 (L2)	0.259	3.80	0.1346
Link 3 (L3)	0.247	3.68	0.0814
Link 4 (L4)	0.383	28.04	2.0281
Link 5 (L5)	0.395	7.48	0.6348
Link 6 (L6)	0.090	1.40	0.0319
Link 7 (L7)	0.100	0.46	0.0006

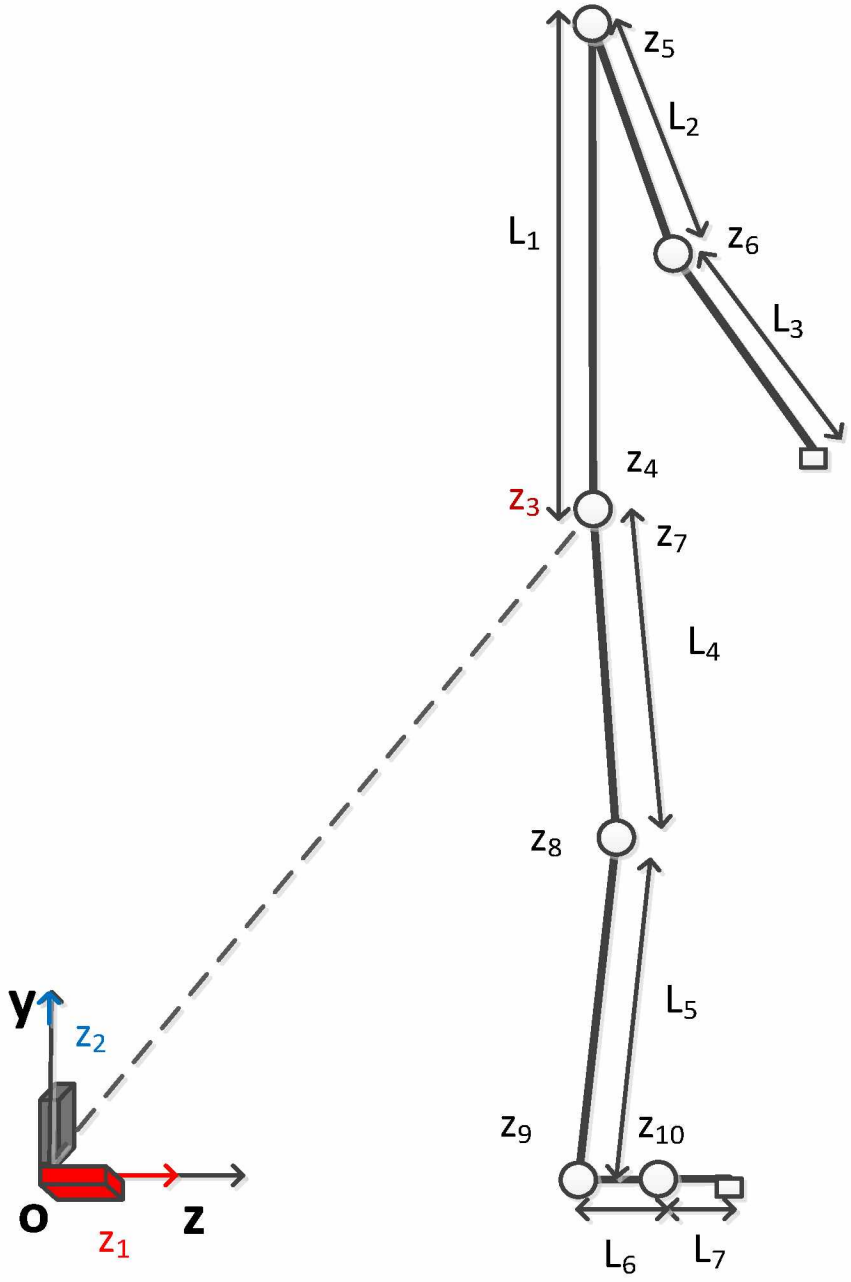

Figure 2. 1 The 2D lifting skeletal model

Figure 2.2 depicts how the global DOF are set up in the Denavit-Hartenberg (DH) method (Denavit, 1955). Each degree of freedom is given in the local z-direction in both the translational joint and the rotational joint. For revolute joint (GR1), the direction of rotation is the *z*-axis according to the right-hand rule. On the other hand, for prismatic joints (GT1 and GT2), the

direction of the movement will be linear towards z-axis. So, θ and d are the joints variables for revolute and prismatic joint respectively. It is noted that the global rotation joint (z_3), spine joint (z_4), and hip joint (z_7) coincide at the same location. The positive directions for all the local rotation joints ($z_3 \sim z_{10}$) are clockwise in global Y-Z plane.

Table 2. 2 Joint angle symbols and names

Symbol	Coordinate name	Symbol	Coordinate name
z_1	Global translation joint coordinate	z_6	Elbow joint coordinate
z_2	Global translation joint coordinate	z_7	Hip joint coordinate
z_3	Global rotation joint coordinate	z_8	Knee joint coordinate
z_4	Spine joint coordinate	z_9	Ankle joint coordinate
z_5	Arm joint coordinate	z_{10}	Subtalar joint coordinate

There are two branches in the body frame with respect to the global coordinate branch (parent): the spine-arm branch and leg branch. In the spine-arm branch, two arms are represented as a single branch since only 2D symmetric lifting is studied. The arm branch includes upper arm and lower arm. In the leg branch, two legs are combined as a single branch including thigh, tibia and foot.

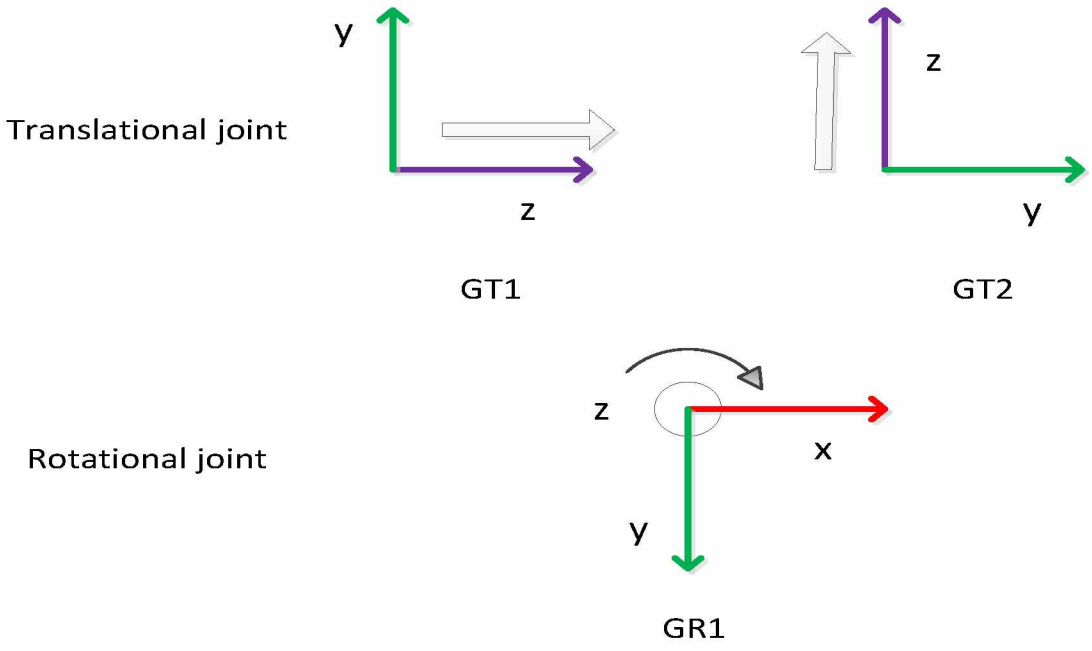

Figure 2. 2 Global degrees of freedom

The DH parameters are described in Table 2.2, where θ represents a rotation about local z-axis, d represents the translational distance on local z-axis, a represents the translational distance on local x-axis, and α represents the rotation on local x-axis. The motion sequence is θ, d, a, and α.

Table 2. 3 DH table for 2D human model

DOF	θ	d	a	α	Segment
GT1	π	0	0	$\pi/2$	global translation
GT2	$\pi/2$	L_1+L_2	0	$-\pi/2$	
GR1 (to leg)	0	0	0	0	global rotation
GR1 (to spine)	0	0	0	0	
Q1	$-\pi/2$	0	L_1	0	spine
Q2	π	0	L_2	0	arm
Q3	0	0	L_3	0	
Q4	$\pi/2$	0	L_4	0	leg
Q5	0	0	L_5	0	
Q6	$-\pi/2$	0	L_6	0	
Q7	0	0	L_7	0	

The kinematics and dynamics are calculated using DH-based recursive Lagrangian approach (Hollerbach, 1980; Toogood, 1989; Xiang, Arora, & Abdel-Malek, 2008). The equation of motions are expressed in Eq. (2.1) – Eq.(2.5), where the first term in the torque expression Eq. (2.1) is the inertia and Coriolis torque, the second term is the torque due to gravity load, the third term is the torque due to external force, and the fourth term represents the torque due to the external moment.

$$\tau_i = \mathrm{tr}\left(\frac{\partial \mathrm{A_i}}{\partial \mathrm{q_i}}\mathbf{D}_i\right) - \mathbf{g}^{\mathrm{T}}\frac{\partial \mathbf{A}_i}{\partial q_i}\mathbf{E}_i - \mathbf{f}_k^{\mathrm{T}}\frac{\partial \mathbf{A}_i}{\partial q_i}\mathbf{F}_i - \mathbf{G}_i^{\mathrm{T}}\mathbf{A}_{i-1}\mathbf{z}_0 \tag{2.1}$$

$$\mathbf{D}_i = \mathbf{I}_i\mathbf{C}_i^{\mathrm{T}} + \mathbf{T}_{i+1}\mathbf{D}_{i+1} \tag{2.2}$$

$$\mathbf{E}_i = m_i\mathbf{r}_i + \mathbf{T}_{i+1}\mathbf{E}_{i+1} \tag{2.3}$$

$$\mathbf{F}_i = \mathbf{r}_k\delta_{ik} + \mathbf{T}_{i+1}\mathbf{F}_{i+1} \tag{2.4}$$

$$\mathbf{G}_i = \mathbf{h}_k\delta_{ik} + \mathbf{G}_{i+1} \tag{2.5}$$

where $tr(\cdot)$ is the trace of a matrix, $\mathbf{A}_i$ and $\mathbf{C}_i$ are the recursive kinematics position and acceleration matrices respectively, q_i is the joint angle, $\mathbf{I}$ is the inertia matrix for link i, $\mathbf{D}_i$ is the recursive inertia and Coriolis matrix, $\mathbf{g}$ is the gravity vector, m_i is the mass of link i, $\mathbf{r}_i$ is the center of mass of link i, $\mathbf{f}_k = [0 \quad f_{ky} \quad f_{kz} \quad 0]^{\mathrm{T}}$ is the external force applied on link k, $\mathbf{r}_k$ is the position of the external force in the local frame k, $\mathbf{h}_k = [h_x \quad 0 \quad 0 \quad 0]^{\mathrm{T}}$ is the external moment applied on link k, $\mathbf{T}_i$ is the link transformation matrix, $\mathbf{z}_0 = [0 \quad 0 \quad 1 \quad 0]^{\mathrm{T}}$ is for a revolute joint, $\mathbf{z}_0 = [0 \quad 0 \quad 0 \quad 0]^{\mathrm{T}}$ is for a prismatic joint, finally, δ_{ik} is Kronecker delta. Although, it is a 2D model, 4x1 matrices are taken to make it homogenous. The detail derivations of $\mathbf{A}_i$ and $\mathbf{C}_i$ are described in Toogood (Toogood, 1989) and Xiang (Xiang et al., 2008).

Chapter 3 Optimization Formulation

Optimization helps to find out the best solution for the redundant design and motion planning problems. The optimal solution is obtained by minimizing or maximizing certain human performance measures based on the equations of motion (EOM) and given constraints. Some constraints are commonly used for all types of tasks, such as joint angle limits and joint torque limits. We will discuss those in basic optimization formulation. Then, we will discuss anew optimization formulation for maximum weight lifting motion prediction.

3.1 Basic optimization formulation

The lifting motion prediction is formulated as an optimization problem in Equation (3.1): find the optimal control points **P** of joint angle profiles for the lifting motion to minimize a human performance measure, $J(\mathbf{P})$, subject to physical constraints g_i as follows:

$$\begin{aligned} &\text{Find:} && \mathbf{P} \\ &\min: && J(\mathbf{P}) \\ &\text{Sub.} && g_i \leq 0, \quad i = 1, \ldots, n \end{aligned} \tag{3.1}$$

where, n is the total number of constraints.

Objective function

In a previous study, the dynamics effort was used as an objective function for the lifting motion which is defined as time integration of all joint torque squared (Yujiang Xiang, Jasbir S. Arora, & Karim Abdel-Malek, 2012; Xiang, Arora, Rahmatalla, et al., 2010).

$$J_1(\mathbf{P}) = \sum_{i=4}^{ndof} \int_0^T \tau_i^2(\mathbf{P})\, dt \tag{3.2}$$

where T is the total lifting time; $ndof$ is the number of DOF. Note that the joint torque for each global DOF is zero for a balanced lifting motion.

Constraints

The general constraints for a 2D symmetric lifting motion include:

(1) Joint angle limits

$$\mathbf{q}^L \leq \mathbf{q}(\mathrm{t}) \leq \mathbf{q}^U \tag{3.3}$$

where $\mathbf{q}^L$ is the lower joint angle limit and $\mathbf{q}^U$ upper limit.

(2) Joint torque limits

$$\boldsymbol{\tau}^L \leq \boldsymbol{\tau}(\mathrm{t}) \leq \boldsymbol{\tau}^U \tag{3.4}$$

where $\boldsymbol{\tau}^L$ is the lower joint torque limit and $\boldsymbol{\tau}^U$ upper limit.

(3) Feet contacting positions

$$\mathrm{P}(\mathrm{feet}, \mathrm{t}) = \mathrm{P}^s_{feet} \tag{3.5}$$

where P^s_{feet} is the specified feet contact position on the level ground.

(4) Balance condition

$$\mathrm{P}(\mathrm{ZMP}, \mathrm{t}) \in \mathrm{FSR} \tag{3.6}$$

where zero moment point (ZMP) position is inside the foot support region (FSR).

(5) Collision avoidance

$$\mathrm{d}(\mathrm{t}) \geq \mathrm{r}_1 + \mathrm{r}_2 \tag{3.7}$$

where d is the calculated distance between the hand and the circle center on body segment representing the body thickness, r_1 is half of the box width and r_2 is the radius of the circle. There are a total of seven circles filled into body segments: two for spine and five for leg.

(6) Initial and final hand positions

$$\mathrm{P}(\mathrm{hand}, \mathrm{t} = 0, T) = \mathrm{P}^s_{hand}(\mathrm{t} = 0, T) \tag{3.8}$$

Where, P^s_{hand} is the specified hand position at initial and final times.

(7) Initial and final velocities

$$\dot{\mathbf{q}}(\mathrm{t}=0,T)=\mathbf{0} \tag{3.9}$$

where the initial and final lifting motions are static.

All these constraints are described in detail in Xiang (Xiang, Arora, Rahmatalla, et al., 2010). The joint angle limits and static joint torque limits are given in Appendix A1 and A2. The following sections will introduce the new optimization formulation including new design variables (lifting weight and time), new objective function (maximum lifting weight), and new constraint (dynamic strength) in detail.

3.2 New optimization formulation

We will consider external force and time grids as design variables and optimize those in the optimization formulation. Also, we will discuss the procedure to apply dynamic joint strength in our predictive model.

3.2.1 External force as design variable

In a previous formulation, the external forces are given as constant, i.e., $\mathbf{f}_k$ and $\mathbf{h}_k$ are constant values in Equations (2.1-2.5). In this study, these external forces could be treated as unknowns (design variables) in the optimization formulation. Therefore, the joint torques from the EOM are not only the function of joint angle control points $\mathbf{P}$, but also the independent external forces. The sensitivity of joint torque with respect to external force should be derived for gradient-based optimization. Without loss of generality, an active external load along vertical direction f_{ky} is treated as a design variable. f_{ky} affects the joint torques in two ways: explicit effect (τ_i^o) from the EOM, and implicit effect ($\tilde{\tau_i}$) from passive ground reaction forces (GRF). The direct differentiation of τ_i^o with respect to f_{ky} can be obtained from Equation (2.1) directly as:

$$\frac{\partial \tau_i^o}{\partial f_{ky}}=[0 \quad 1 \quad 0 \quad 0]\frac{\partial \mathbf{A}_i}{\partial q_i}\mathbf{F}_i \tag{3.10}$$

However, the external force, GRF, also depends on f_{ky} passively due to balance condition. For inverse dynamics formulation, the GRF is calculated from global joint torques using an active-passive balance algorithm (Xiang, Arora, Rahmatalla, & Abdel-Malek, 2009) as shown in Figure 3.1 Therefore, $\mathbf{f}^{GRF} = [0, \quad f_y^{GRF}(\tau_{1\sim3}^o), \quad f_z^{GRF}(\tau_{1\sim3}^o), \quad 0]^{\mathrm{T}}$ is a function of $\tau_{1\sim3}^o$ (active global joint torques). Then the sensitivity of joint torque $\tau_i^{\sim}$ with respect to f_{ky} due to GRF is calculated using chain rule as:

$$\frac{\partial \tau_i^{\sim}}{\partial f_{ky}} = \frac{\partial \tau_i^{\sim}}{\partial f_y^{GRF}} \frac{\partial f_y^{GRF}}{\partial \tau_{1\sim3}^o} \frac{\partial \tau_{1\sim3}^o}{\partial f_{ky}} + \frac{\partial \tau_i^{\sim}}{\partial f_z^{GRF}} \frac{\partial f_z^{GRF}}{\partial \tau_{1\sim3}^o} \frac{\partial \tau_{1\sim3}^o}{\partial f_{ky}} \tag{3.11}$$

$$\frac{\partial \tau_i^{\sim}}{\partial f_y^{GRF}} = [0 \quad 1 \quad 0 \quad 0] \frac{\partial \mathbf{A}_i}{\partial q_i} \mathbf{F}_i \tag{3.12}$$

$$\frac{\partial \tau_i^{\sim}}{\partial f_z^{GRF}} = [0 \quad 0 \quad 1 \quad 0] \frac{\partial \mathbf{A}_i}{\partial q_i} \mathbf{F}_i \tag{3.13}$$

where the term $\frac{\partial f_y^{GRF}}{\partial \tau_{1\sim3}^o}$ involves ZMP location. Refer to Xiang et al. (Xiang, Arora, Rahmatalla, & Abdel-Malek, 2009) for detailed calculations. The term $\frac{\partial \tau_{1\sim3}^o}{\partial f_{ky}}$ is obtained from Equation (3.10). Finally the sensitivity of joint torque with respect to the active external load f_{ky} is the summation of Equations (3.10) and (3.11):

$$\frac{\partial \tau_i}{\partial f_{ky}} = \frac{\partial \tau_i^o}{\partial f_{ky}} + \frac{\partial \tau_i^{\sim}}{\partial f_{ky}} \tag{3.14}$$

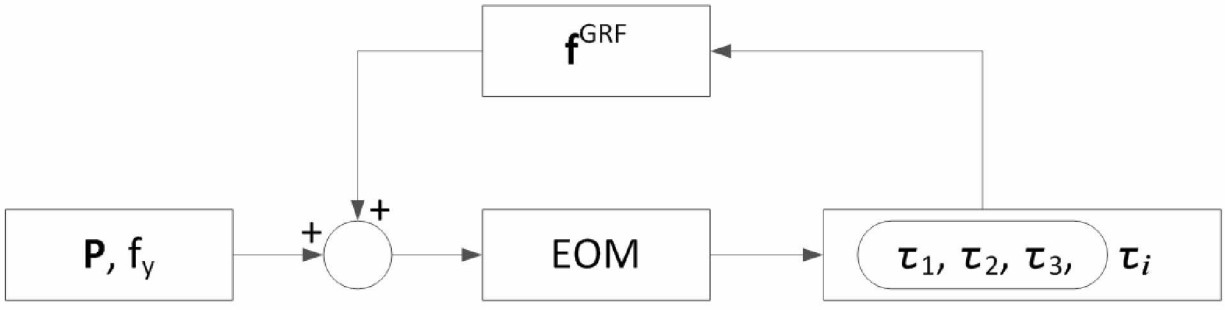

Figure 3. 1 GRF active-passive feedback flowchart

By treating external forces as design variables in the optimization formulation, we can define $W = -f_y$ as the weight of a box applied downward on hand (f_y is negative). The new objective function to maximize the lifting weight is defined as:

$$J_2(\mathbf{P}, W) = -W \tag{3.15}$$

Note that the negative sign is to convert a maximization problem into a minimization problem.

3.2.2 Time grid points as design variables

The optimization problem is formulated as a nonlinear programming (NLP) using cubic B-spline discretization. Thus a joint angle profile $q(t)$ is parameterized as follows:

$$q_i(\mathbf{t}, \mathbf{P}) = \sum_{j=1}^{4} N_j(\mathbf{t}) p_{ij} \tag{3.16}$$

Where $N_j(\mathbf{t})$ are the basis functions, $\mathbf{t} = \{t_0, \ldots, t_s\}$ is the knot vector (time grid), and $\mathbf{P}_{ij} = \{p_{i0}, \ldots, p_{im}\}$ is the vector of control points for the i th joint angle profile and $m+1$ is the number of control points.

The gradients of state variables with respect to the kth knot variable are derived as:

$$\frac{\partial q_i}{\partial t_k} = \sum_{j=1}^{4} \frac{\partial N_j(\mathbf{t})}{\partial t_k} p_{ij} \tag{3.17}$$

$$\frac{\partial \dot{q}_i}{\partial t_k} = \sum_{j=1}^{4} \frac{\partial \dot{N}_j(\mathbf{t})}{\partial t_k} p_{ij} \tag{3.18}$$

$$\frac{\partial \ddot{q}_i}{\partial t_k} = \sum_{j=1}^{4} \frac{\partial \ddot{N}_j(\mathbf{t})}{\partial t_k} p_{ij} \tag{3.19}$$

Thus, the joint torque gradient with respect to the kth knot variable is derived as:

$$\frac{\partial \tau_i}{\partial t_k} = \sum_{j=1}^{ndof} \left(\frac{\partial \tau_i}{\partial q_j} \frac{\partial q_j}{\partial t_k} + \frac{\partial \tau_i}{\partial \dot{q}_j} \frac{\partial \dot{q}_j}{\partial t_k} + \frac{\partial \tau_i}{\partial \ddot{q}_j} \frac{\partial \ddot{q}_j}{\partial t_k} \right) \tag{3.20}$$

where the sensitivity of joint torque with respect to state variables are obtained from the reference (Xiang et al. 2009b), in which GRF feedback loop in Figure 3.1 is used to calculate joint torque.

3.2.3 Dynamic joint strength

In literature (Frey-Law et al., 2012; Sara J Hussain & Laura Frey-Law, 2016; Looft, 2014; Stockdale, 2011), the dynamic isokinetic and isometric strengths of ankle, knee, hip, spine, shoulder, and elbow were tested using experiments through a normal range of motion. The peak torque for a given joint position and angular velocity was measured. These data can be used to model joint dynamic strength surface as a function of joint angle and angular velocity. In this section, a surrogate model is developed from the experimental data. The logistic equations are used to model the peak torque as a function of both joint angle and angular velocity, and the coefficients of the logistic function are obtained from Gauss least square regressions. The corresponding peak torque-angle-velocity relationship is given as:

$$\tau_{\text{peak}} = c_1 + c_2 \frac{4e^{-(q-c_3)/c_4}}{[1+e^{-(q-c_3)/c_4}]^2} + c_5 \frac{4e^{-(v-c_6)/c_7}}{[1+e^{-(v-c_6)/c_7}]^2} + c_8 \frac{4e^{-(q-c_3)/c_4}}{[1+e^{-(q-c_3)/c_4}]^2} \frac{4e^{-(v-c_6)/c_7}}{[1+e^{-(v-c_6)/c_7}]^2} \quad (3.21)$$

where $c_1 \sim c_8$ are regression equation coefficients, e is the exponential function, q is the joint angle, and v is the joint angular velocity. The coefficients in Equation (3.21) are scaled mean values, and along with the coefficients covariance (CV) determined with each curve fit. Therefore, a specific percentile strength can be determined as follows:

$$\tau_{\text{peak}}^{\%} = p * \text{CV} * \tau_{\text{peak}} + \tau_{\text{peak}} \quad (3.22)$$

where p is the percentile.

This surrogate model is then used to develop the joint dynamic strength constraints for lifting motion optimization. Since joint torque value has both positive and negative directions, the torque peak value in Equation (3.21) needs to be developed separately in each direction to obtain τ_{peak}^{L} (negative) and τ_{peak}^{U} (positive). Finally, the joint torque constraint is imposed as:

$$0 \leq \frac{\tau(t) - \tau_{\text{peak}}^{L}(t)}{\tau_{\text{peak}}^{U}(\text{t}) - \tau_{\text{peak}}^{L}(t)} \leq 1 \quad (3.23)$$

In this study, the dynamic strengths are modeled for ankle, knee, hip, spine, shoulder, and elbow joints. The experimental data are obtained from the literature (Frey-Law et al., 2012; Sara J. Hussain & Laura Frey-Law, 2016; Looft, 2014; Stockdale, 2011). Considering external force and time grid as design variables and adding a dynamic joint strength constraint will help us to predict the maximum weight, the optimal time duration, and the lifting motion simultaneously. We will discuss this in the next chapter.

Chapter 4 Maximum Weight Prediction

Maximum lifting weight is a vital factor for manual material handling. NIOSH has some lifting equations based on static joint strength. In real life, however, human joint strength is dynamic. Maximum lifting weight can be predicted from dynamic strength based motion prediction model. The total lifting time duration is uniformly discretized into twelve segments. There are total 52 design variables (50 control points + 1 for W + 1 for T) and 511 nonlinear constraints for the symmetric lifting motion optimization. The SQP-based optimizer, SNOPT (Gill, Murray, & Saunders, 2002), is used to solve the optimization problem. This dynamic joint strength based formulation is very efficient (Ackermann & Van den Bogert, 2010; Fregly et al., 2007; Ren et al., 2007).

In this section, we predict the maximum lifting weight, time duration, and lifting motion by considering the dynamic strength constraints. The maximum weight objective function Eq. (3.15) is used in the optimization formulation with the given initial and final box locations. We simulate a lifting that moves a box from the initial location ($y_1 = 0.2$ m, $z_1 = 0.35$ m) to the final location ($y_2 = 1.0$ m, $z_2 = 0.46$ m). Note that y is the vertical height measured from hand to ground, and z is the horizontal distance measured from hand to ankle. The dynamic strengths of all joints are considered in the optimization. The initial and final postures are also optimized along with the lifting motion. The initial guess for design variables are $\mathbf{P} = \mathbf{0}, W = 50$ N, $T = 1.0$ s; the optimal solutions are $W = 493.68$ N, $T = 0.708$ s. The joint torque profiles for the maximum weight lifting are illustrated in Figure 4.1. The stick diagram of the predicted maximum weight lifting motion is depicted in Figure 4.2. The optimal solution is obtained in 5.86 seconds CPU time.

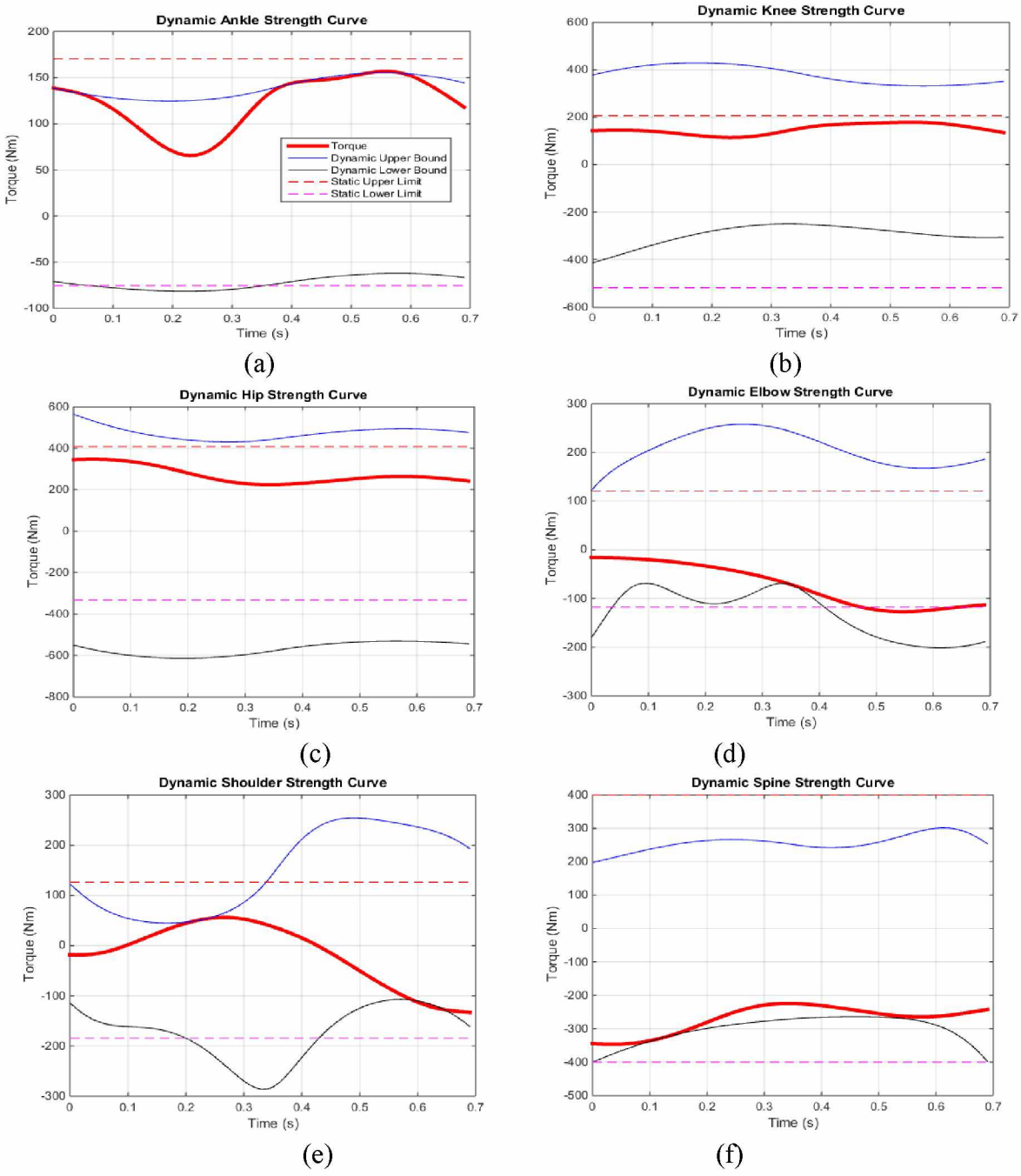

Figure 4. 1 Joint torque profiles for the maximum weight lifting: (a) ankle, (b) knee, (c) hip, (d) elbow, (e) shoulder, and (f) spine

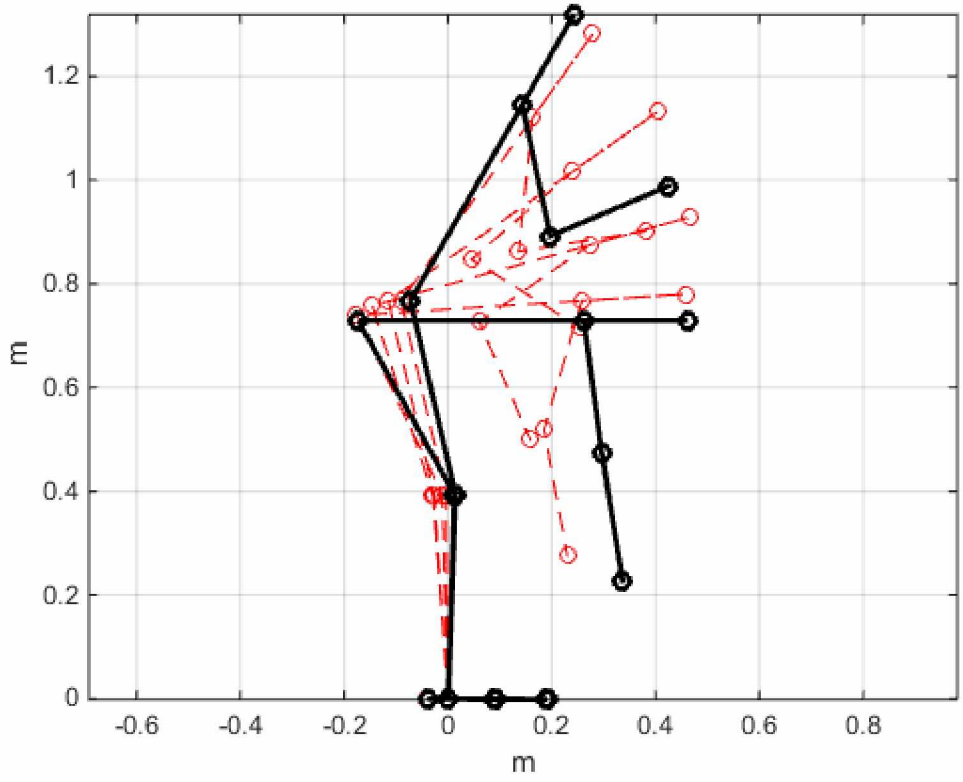

Figure 4. 2 Snapshots of the maximum weight lifting motion

From the simulation results we can see that the ankle, elbow, shoulder, and spine dynamic strength are activated. The knee and hip torques are close to their static strength limits and the dynamic strengths are not activated. From Figure 4.2, we can see that for the maximum weight lifting, knee is not fully used with less flexion. This means the box weight is mainly carried by the upper limb and limited by its dynamic strength. This strategy also depends on the given initial and final box locations.

To find out the maximum lifting weight, the algorithm predicts back lifting strategy with little ankle movement for the given strength and box locations in Figure 4.2. This strategy seems contradictory to real-world ergonomic experience: for heavy objects, people use squat lifting and for lightweight objects, they use back lifting, and squat lifting may lift more weight. The back lifting strategy for maximum weight lifting is predicted in this study because the box is initially

placed far from the body. This results in a large torque on ankle joint at initial posture when lifting a heavy box. For further illustration, we plot the ankle joint dynamic strength curve with zero velocity, which corresponds to static initial condition shown in Figure 4.3.

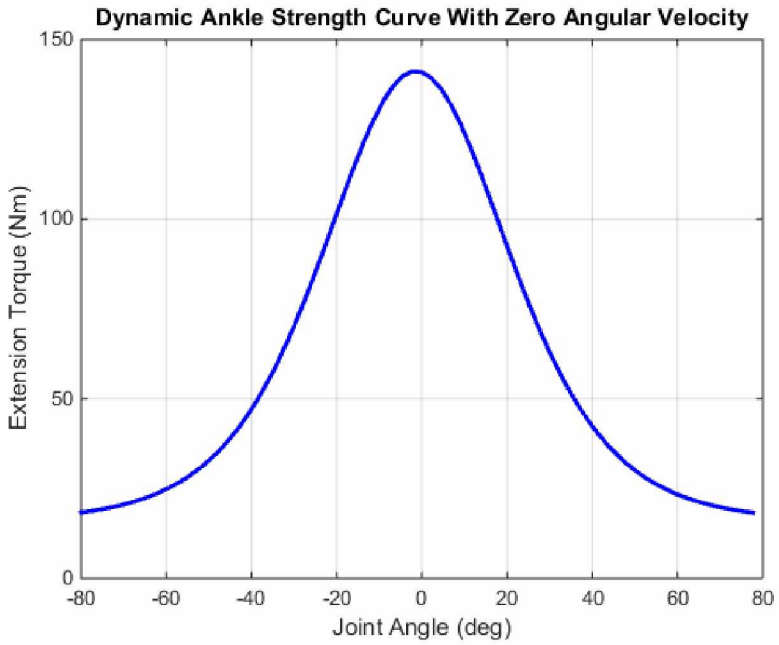

Figure 4. 3 Ankle extension strength with zero velocity for the maximum weight lifting

The graph in this figure shows that the ankle is strongest at around zero degrees, demonstrating that if people use the squat lifting strategy to lift a heavy object positioned far from the body, they may fall over because of weaker ankle strength at a flexion angle (squat). It is seen in Figure 4.1 that many joint dynamic strengths are activated except for hip and knee joints. This depends on the predicted lifting strategy: the upper limb is fully activated to move the heavy object to the destination, but the lower limb is not fully used due to the weaker ankle joint. Initially, the ankle joint has to find an optimal angle to take the heavy weight statically because lifting is constrained to be static at initial and final time locations. In this case, the ankle joint angle is very small, around zero value. It appears that the given box location greatly affects the predicted maximum lifting weight. If the box's initial distance is closer to the body, the torque generated by the box on the ankle is small. The ankle and knee are able to flex to facilitate a squatting heavy-

weight-lifting motion, which might lift more weight using knee and hip joints. An ideal formulation is to treat the initial and final box distances as additional design variables in the optimization formulation to predict the maximum weight-lifting strategy. Therefore, it is critical to consider the dynamic strength in predicting the maximum lifting weight since heavy objects could easily activate dynamic strength.

Chapter 5 OpenSim Simulation for Maximum Weight Lifting

5.1 OpenSim

OpenSim is an open source software application for visualizing musculoskeletal structures and simulating movements of human and animals. The application includes various tools to compute inverse kinematics and dynamics, residual reduction algorithm to eliminate tracking error, computed muscle control to analyze muscles, methods to create simulation from motion capture and optimization to estimate muscle and joint forces. OpenSim 3.0 is based on 3 muscle models. Those are the Thelen 2003 Muscle model (Thelen, 2003; Thelen, Anderson, & Delp, 2003), Millard 2012 Equilibrium model, and Millard 2012 Acceleration model (Matthew Millard, Thomas Uchida, Ajay Seth, & Scott L. Delp, 2013).

5.2 OpenSim simulation and processing

An existing generic model of OpenSim will be used to visualize human movement. Before that, anthropometry of the simulation model and OpenSim model should be same. Scaling is very important before inserting data in computed muscle control (CMC) because the solutions are very sensitive to the accuracy of the scaling step. To do the scaling, the Scale Tool in OpenSim is used to match the anthropometry of generic OpenSim model with our simulation model.

To insert experimental data in OpenSim directly from laboratory, marker points, scaling, inverse kinematics (IK) and residual reduction algorithm (RRA) are used. In contrast, from our predictive simulation model, the state variables ($q, \dot{q}, \ddot{q}$), joint torque (τ), ground reaction forces (GRF) and external forces (F_{ex}) are available and can be inserted to OpenSim directly. By inserting these parameters, muscle excitation, activation and forces can be found using computed muscle control algorithm.

Computed muscle control (CMC) is based on Thelen's work (Darryl G Thelen & Frank C Anderson, 2006) for generating muscle actuated simulations of human movements. It can compute muscle excitation level (full excitation is 1 and no excitation is 0) which ultimately derive the generalized coordinates such as joint angles towards a desired trajectory. Computed muscle control needs three steps to calculate muscle force, activation, and excitation.

1. Compute desired acceleration
2. Static optimization
3. Forwards Dynamics

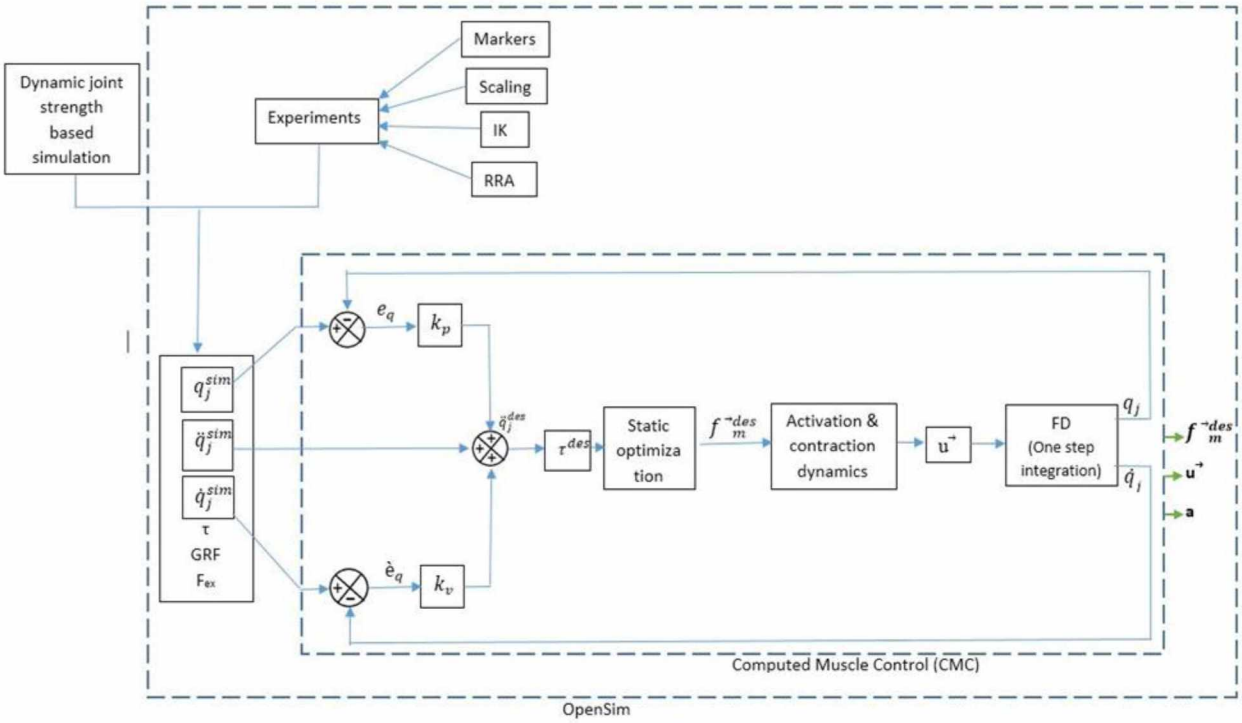

Figure 5. 1 Computed muscle control (CMC) flow chart

The first step of CMC is to compute desired accelerations ($\ddot{q}_j^{des}(t+T)$) based on Proportion-Derivative (PD) control. This will derive generalized coordinates (q_j) and speeds ($\dot{q}_j$)

towards our simulaiton based kinematics (q_j^{sim} and $\dot{q}_j^{sim}$). k_p and k_v are feedback gains that carry the current position error (e_q) and velocity ($\dot{e}_q$) error. So, from Figure 5.1, it can be written

$$\ddot{q}_j^{des}(t+T) = \ddot{q}_j^{sim}(t+T) + k_v[\dot{q}_j^{sim}(t) - \dot{q}_j(t)] + k_p[q_j^{sim}(t) - q_j(t)] \qquad (5.1)$$

If we consider,

$$\dot{q}_j^{sim}(t) - \dot{q}_j(t) = \dot{e}_j \; and \; q_j^{sim}(t) - q_j(t) = e_j, \qquad (5.2)$$

Then Eq. (5.1) will be:

$$\ddot{q}_j^{des}(t+T) = \ddot{q}_j^{sim}(t+T) + k_v \dot{e}_j + k_p e_j \qquad (5.3)$$

To track our simulation coordinates (q_j^{sim}) in OpenSim, based on the tracking errors ($\dot{e}_j$ & e_j) and simulated acceleration ($\ddot{q}_j^{sim}$) at time t, the desired joint angle accelerations ($\ddot{q}_j^{des}$) can be computed at time $(t+T)$ using Eq. (5.3), where T is a short interval (T is typically 0.001s). In next step, from the desired accelerations $\ddot{q}_j^{des}(t+T)$, desired torque (τ^{des}) can be found which work as the input for static optimization. Static optimization is used to find out the desired muscle force f_m^{des}. Static optimization distributes net joint torque into muscle tendon forces at instant time. Static optimization computes muscle forces to minimize the cost function J which reduce muscle activations (Thelen 2006). Muscle tendon lengths were used in muscle activation and contraction dynamics to estimate the lower ($f_{m,min}$) and upper ($f_{m,max}$) bound of muscle tendon forces at time ($t + T$). Then the desired muscle force f_m^{des} is used to calculate the muscle excitations (u) as a root-finding problem through muscle excitation and contraction dynamics. The range of muscle excitation is 0 (no excitation) $\leq u \leq 1$ (full excitation).

The next step of computed muscle control is forward dynamics. Muscle excitation, which we

obtained from the desired muscle tendon forces, will be used in forward dynamics to drive the simulation model using one step numerical integration. Therefore, we can get the state variables (q and $\dot{q}$) which will be used in the PD control feedbacks in the first step.

Finally, from this feedback based computed muscle control algorithm, desired muscle force $\boldsymbol{f}_{\boldsymbol{m}}^{\boldsymbol{des}}$, muscle excitations ($\boldsymbol{u}$), and activation $\boldsymbol{a}$ can all be retrieved from the simulation. Meanwhile, the musculoskeletal model of OpenSim can show the simulation movements.

5.3 Data processing

To generate the simulation in OpenSim, it needs either marker trajectories or joint angle profiles, and ground reaction forces, external loads, and centers of pressure data. OpenSim accepts 3 types of data as its input: Maker or Track Row Column (.trc) files, Motion (.mot) files, and Storage (.sto) files. Marker trajectories have to be specified in .trc files. Ground reaction force (GRF) and center of pressure data have to be specified in .sto or .mot files. Joint angles have to be specified in .sto or .mot files. To input experimental EMG data in OpenSim, it has to be imported using .sto or .mot files.

To insert data from our predictive model to OpenSim, we will use .mot (motion) file format which was created by the developers of SIMM (Software for Interactive Musculoskeletal Modeling). The .mot file consists of two parts: The motion header and the data. The first line of motion header is the name, second line is number of rows (nRows) and third line is number of columns (nColumns).

The data taken from real life, for every set of coordinates (x, y and z) are relative to some coordinate system. This coordinate system is called Laboratory coordinate system or Laboratory coordinates. Normally, laboratory coordinate system is fixed to earth. Before putting any value

from laboratory coordinate system to OpenSim, all coordinates (x, y and z) have to be transformed to the particular model coordinate system of OpenSim.

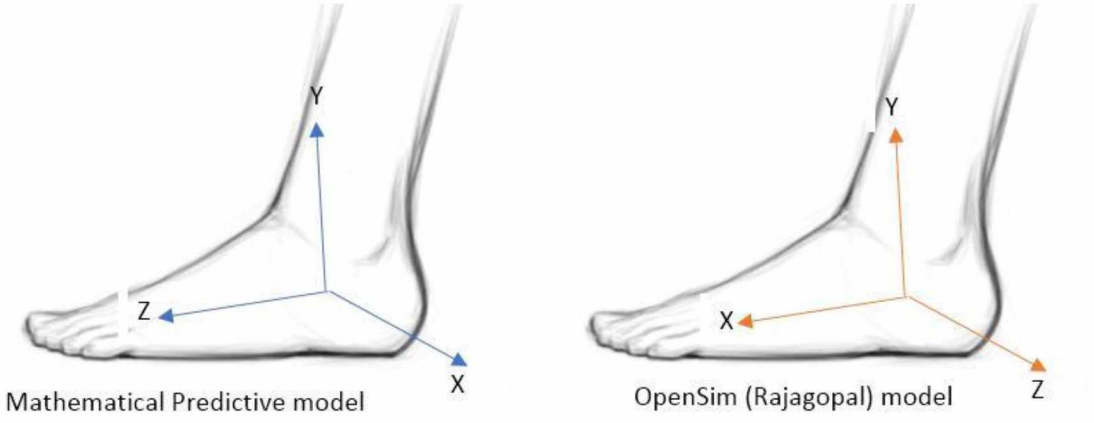

Figure 5. 2 Comparison of coordinates (x, y and z) between Mathematical Predictive model and OpenSim model

For both predictive simulation model and OpenSim model, the center of the coordinate system is halfway between its feet. But, from Figure 5.2 it can be seen that in predictive model, the x-axis points to the left of the model, the y-axis points upward and z-axis points forward from the model. In the OpenSim Raja Gopal Model, the y- axis points upward like the predictive model, but instead of z-axis, x-axis points forward and z-axis points towards left. So, the variables need to be modified for z-axis and x-axis before inserting its value in OpenSim.

5.4 Post processing and analysis

After interfacing predictive model with OpenSim musculoskeletal model, we will get the exact movement like we did in our previous chapter. But, this time we can observe various muscle-tendon length, force, torque, total fiber force, active fiber-force, and passive fiber force.

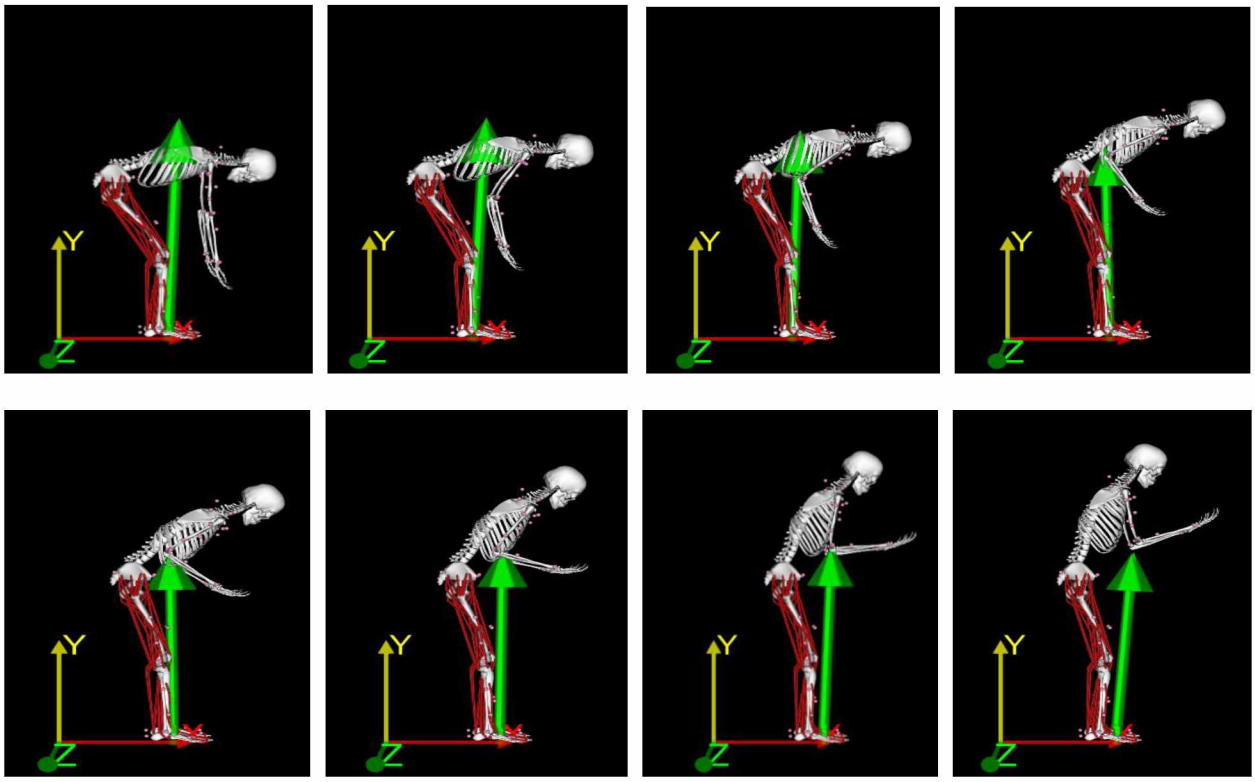

Figure 5. 3 Human body simulation in OpenSim (Side view)

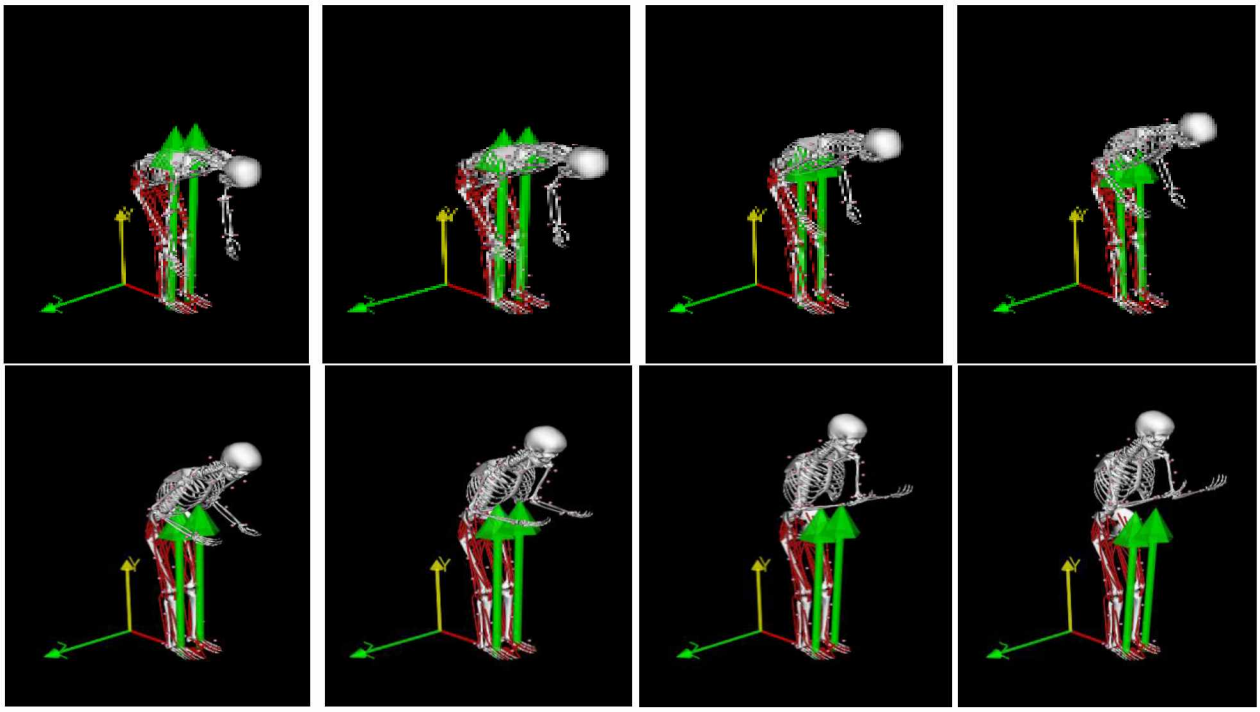

Figure 5. 4 Human body simulation in OpenSim (Isometric view)

During lifting of an object, we extend the knee and hip joints. Also, we can see from Figures 5.3 and 5.4 that the initial ground reaction force was little bit high, then it decreases and finally increases again. It needs high torque initially to lift the weight. It also needs extra torque to decelerate the hand as well as the weight, which leads to high ground reaction force at the end. Also, the direction of the ground reaction force changes continuously to balance the body.

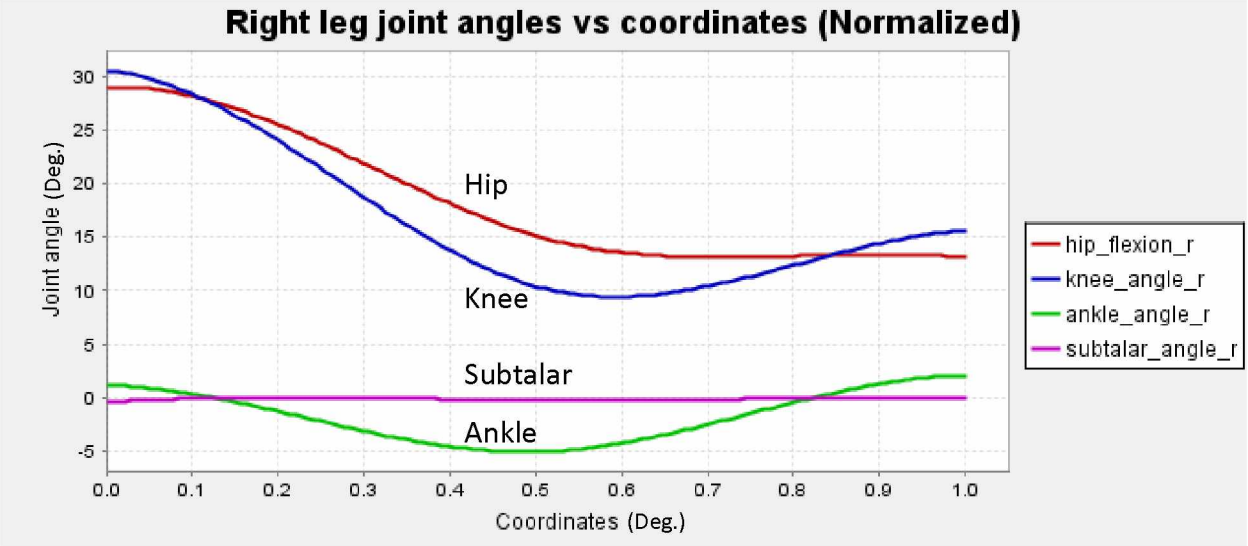

Figure 5. 5 Right leg joint angles vs coordinates

The abbreviation of the muscles name are given below-

Table 5. 1 Muscles name in short-form

bfsh_r	bicep femoris
gaslat_r	gastrocnemius lateralis
gasmed_r	gastrocnemius medialis
grac_r	gracilis
recfem_r	rectus femoris
sart_r	sartorius
vasint_r	vastus intermedius
, vaslat_r	vastus lateralis
vasmed_r	vastus medialis

If we analyze the lower body joint angles, we can see from Figure 5.5 that hip, knee and ankle joint vary a lot, and hip joint remain almost constant after some time. But, knee and ankle joint angle were changed till the end to keep the body stable.

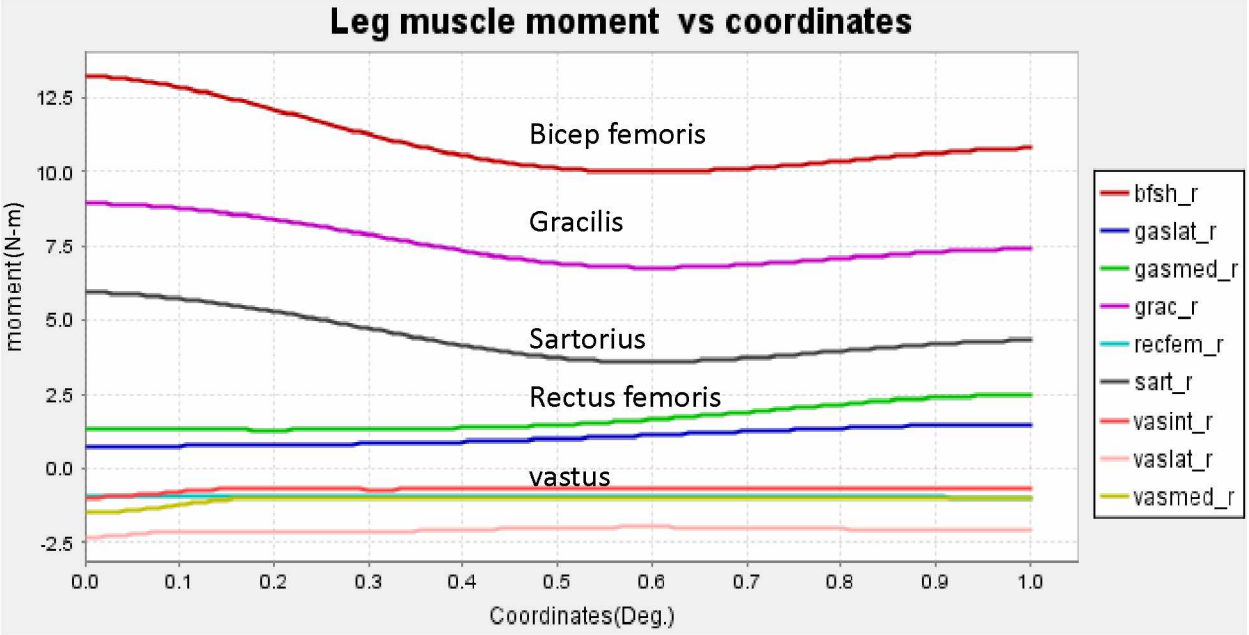

Figure 5. 6 Right leg muscles moment vs coordinates

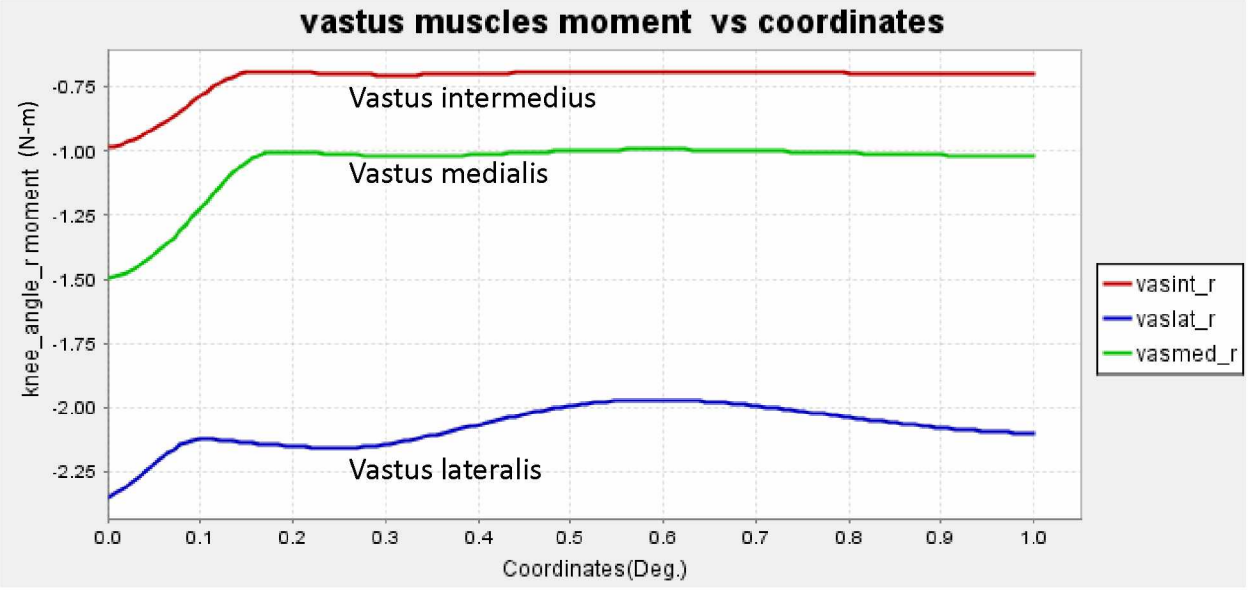

Figure 5. 7 Vastus muscles moment vs. coordinates

We can observe important leg muscles from Figures 5.6 and 5.7 that indicate bicep femoris (short head), gracilis, sartorius, and vastus are the main contributing muscles for the initial moment. From Figure 5.6, we can see that these are thigh muscles near the femur.

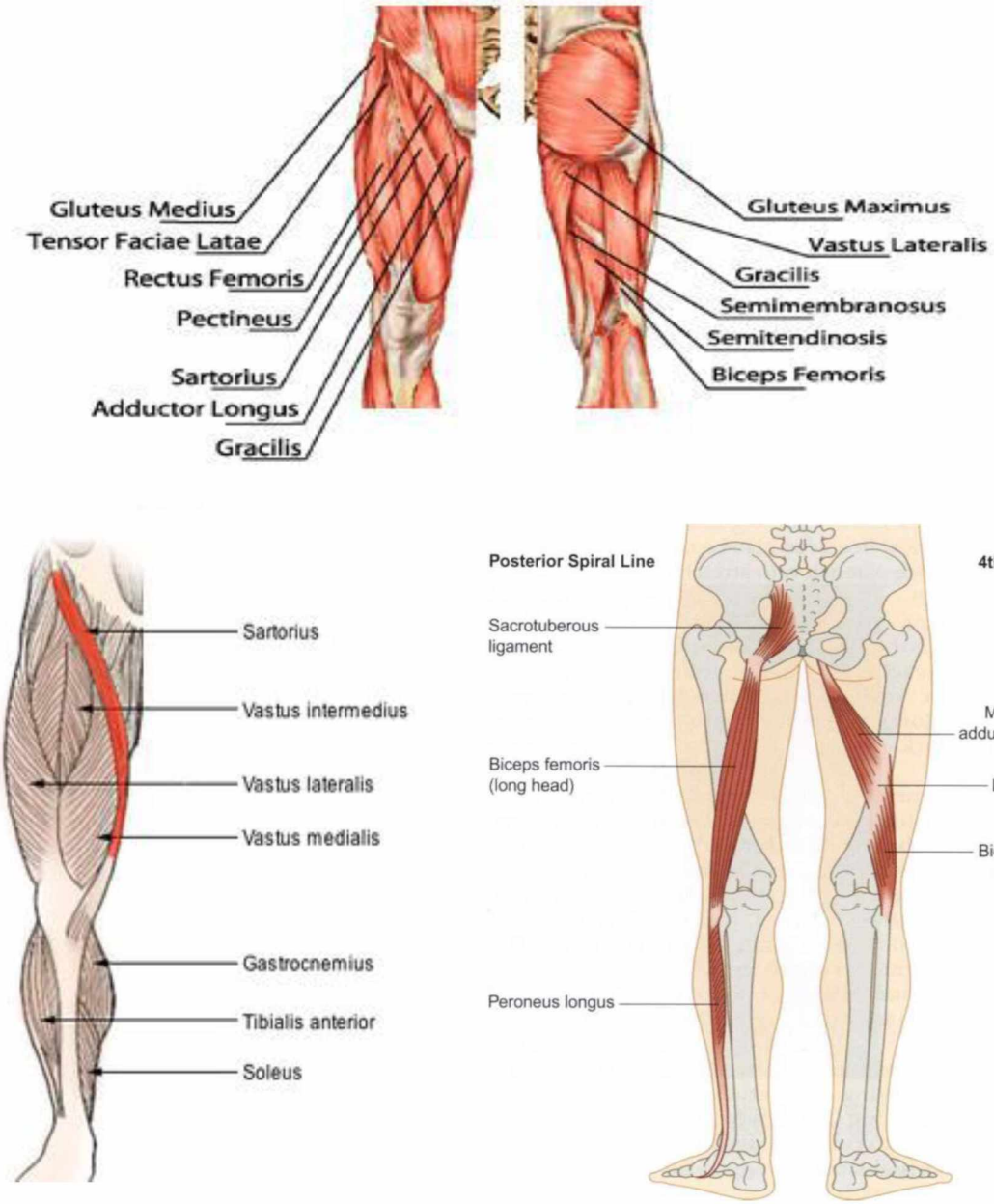

Figure 5. 8 Leg muscles (Bermosa, 2010; Dooley, 2018; "Muscle Contraction and Locomotion,")

If we analyze the normalized fiber length, we can see from Figure 5.9 that there is a significant change of fiber length for vastus, bicep femoris short head, gracilis, and sartorius.

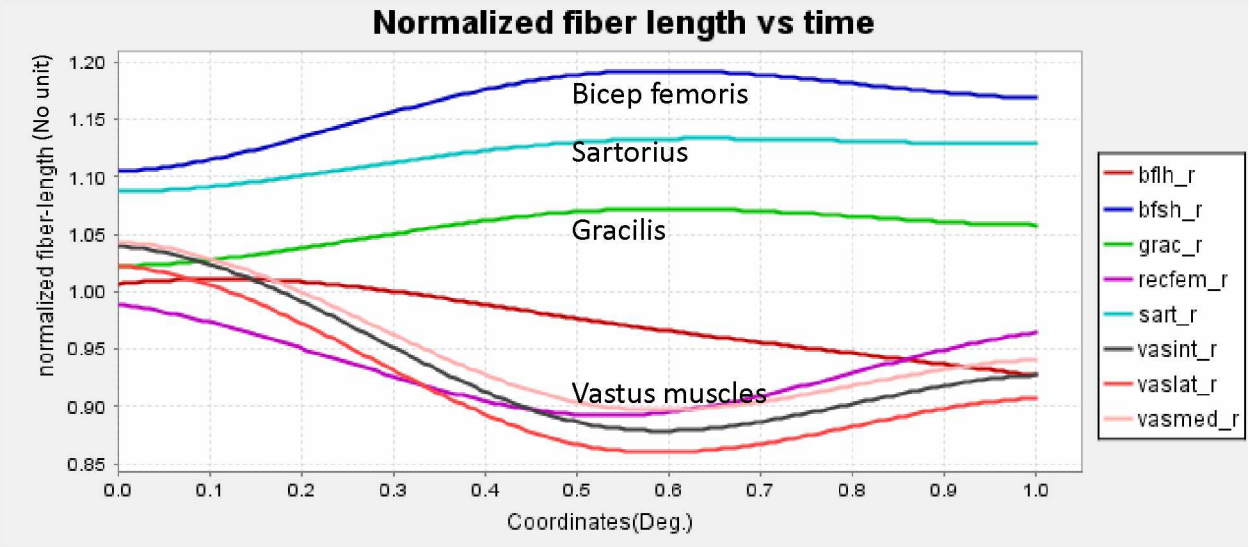

Figure 5. 9 Normalized fiber length vs time for leg muscle

We can analyze the passive fiber force of leg muscles which is responsible for the elasticity of those muscles. We can see that at the beginning of lifting weight, vastus muscles are giving significant amount of force to stand straight. On the other hand, whole time bicep femoris short head is giving maximum passive fiber force.

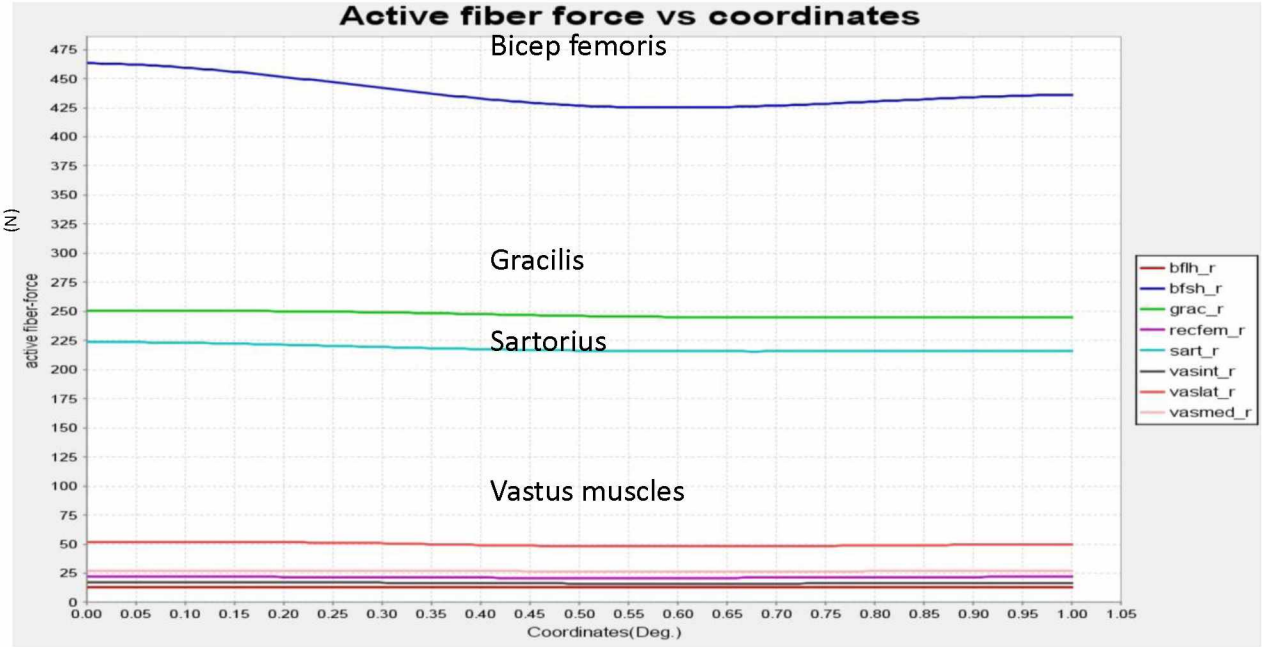

Figure 5. 10 Active fiber force vs coordinates for leg muscle

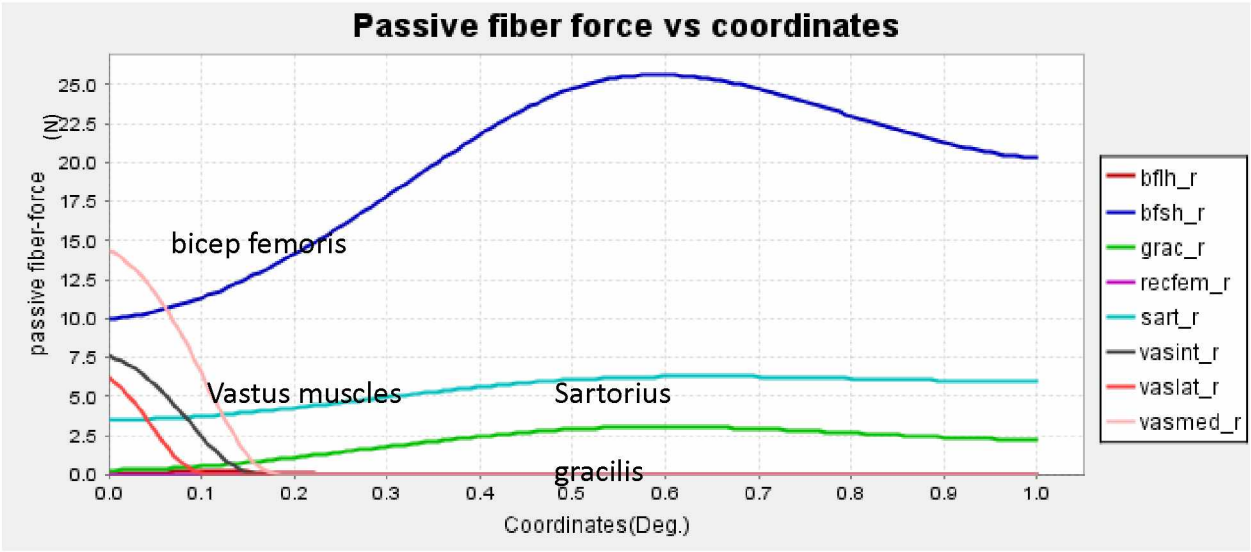

Figure 5. 11 Passive fiber force vs coordinates for leg muscle

If we observe the fiber force in Figure 5.10 and Figure 5.11, it can be seen that mainly passive forces are the main source of motion. Ratcheting mechanism of actin and myosin head is the source of active energy. On the other hand, fiber and connective tissues of a muscle like Epimysium, Perimysium, Endomysium etc. are the main source of passive muscle fiber force. From Figure 5.11 it can be seen that the connective tissue of vastus and later bicep femoris short

head are giving maximum passive force. During the lifting of an extreme heavy load, there is a probability for vastus and bicep femoris muscles to be overloaded and get injured. Bicep femoris is a part of hamstring. It is very common for hamstring to get injured during lifting. That's why we will measure electromyography data for the important leg muscles we have discussed here; specially vastus and bicep femoris for a regular weight lifting, which will be discussed in the next chapter.

5.5 Results and comparison

Using OpenSim, we can not only obtain muscle forces, but also decide which muscles need to be focused on and analyzed for a particular motion. Based on this information we can set our EMG sensors to analyze those muscles instead of analyze all the muscles around the limb for a particular motion. But, for some muscles like rectus femoris, it is not possible to take EMG data as it is an internal muscle of thigh, which is close to the femur. Also, OpenSim cannot predict a motion. If we can develop a predictive model including muscle activation and contraction dynamics, it can help us to analyze those internal muscles.

Chapter 6 Validation of Electromyography

6.1 Electromyography

Electromyography (EMG) is a technique to collect muscle response using biomedical instruments. EMG data represent muscle response or electrical activity produced by skeletal muscles. Electromyography data are collected using tiny devices called electrodes to transmit or detect electrical signals from muscle. EMG data help us to diagnosis neuromuscular disorders like carpal tunnel syndrome, pinched nerve, radiculopathy, muscle diseases, muscular dystrophy etc. Also, it shows a way to train up a particular disordered muscle by observing and analyzing its feedback. In this chapter, we will use EMG data to analysis leg muscles during lifting various weight and try to find out which are the sensitive muscles for lifting weight.

6.2 Experimental setup

Two healthy human subjects with no chronic pain and age range from 24 to 26 participated in this experiment. During all trials, we used six surface electromyography bipolar electrodes (Figure 6.1). We used Trigno Wireless System, Delsys Inc. for our study. The EMG signals were recorded from six leg muscles: vastus medialis, vastus lateralis, vastus, rectus femoris, bicep femoris, gastrocnemius medial head and gastrocnemius lateral head. The EMG signal sampling rate is 2000 samples/sec. Given that the analog signals have a bandwidth of 20 to 450 Hz, such a sampling rate is sufficient to avoid aliasing per the Nyquist theorem.(Jakobsen, Sundstrup, Andersen, Aagaard, & Andersen, 2013). The dimension of the probes is 27 x 37 x 15 mm. The common mode rejection ratio (CMRR) was higher than 80 dB.

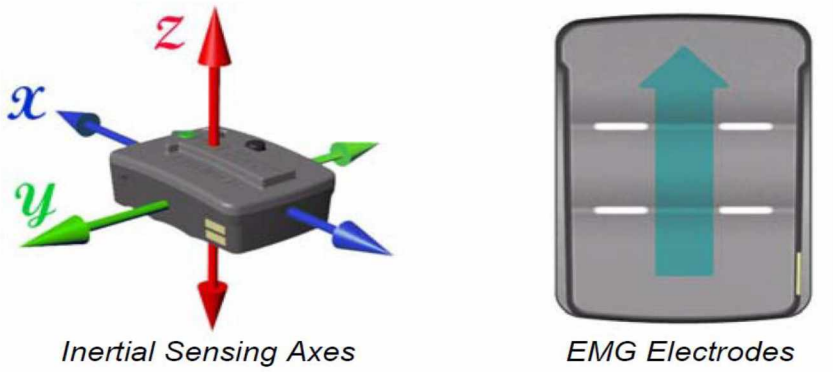

Figure 6. 1 Trigno Wireless 4-channel sensor

6.3 Procedure

EMG data collection and filtering are done by six steps. These steps are followed for all type of weight. The steps are:

Step 1 (Cleaning): Shaving of the hair on skin where the electrode was placed were performed if necessary. The skin area was cleaned with 70% isopropyl alcohol to remove oil or surface residue.

Step 2 (Attaching sensors): To reduce EMG signal cross-talk between muscles, the electrodes were positioned within the border of the muscles and in parallel arrangement to the muscle fibers (Ekstrom, Donatelli, & Carp, 2007). Trigno EMG sensors employ 4 silver-bar contacts for detecting the EMG signal at the skin surface. To obtain the maximum signal amplitude, it is important to place those bars perpendicular to the muscle finer direction like in Figure 6.3. The sensor is placed in the center of the muscle belly and away from tendons or edges of the muscle.

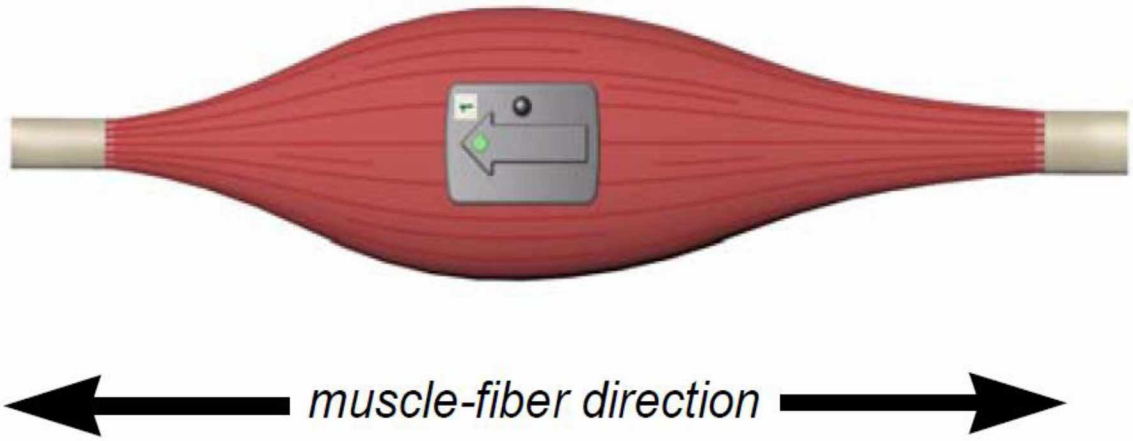

Figure 6. 2 Sensor's arrow with the direction of underlying muscle fibers

Specially designed hype-allergenic adhesive interfaces are used to promote a high quality electrical connection between the sensor bars and the skin ("TRIGNO Wireless System User's Guide," 2014).

The EMG sensors were place on the right leg of each subject. We placed the sensors on vastus medialis, rectus femoris, vastus lateralis, bicep femoris, gastrocnemius medial head and gastrocnemius lateral head. We took the EMG data from these muscle groups during lifting various loads.

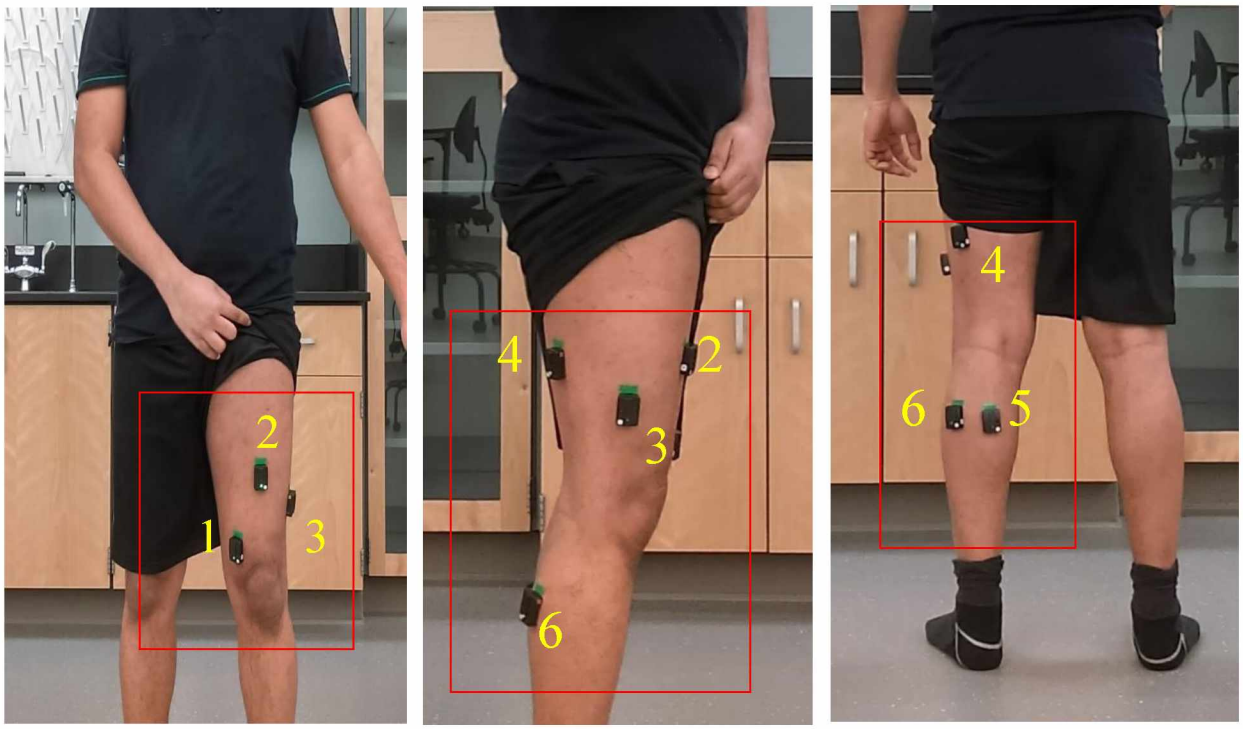

Figure 6. 3 EMG sensor positions

Here, EMG1 represents vastus medialis, EMG2 represents rectus femoris, EMG3 represents vastus lateralis, EMG4 represents bicep femoris, EMG5 represents gastrocnemius medial head and EMG 6 represents gastrocnemius lateral head.

Step 3 (MVC): Maximum Voluntary Contraction (MVC) or Maximum Voluntary Isometric Contraction (MVIC) is needed to normalize the data later. When joints angle is changed during muscle contraction, it is called Isokinetic contraction. On the other hand, when joints angle is kept fixed, it is called Isometric Contraction. Each subject participated in several testing sessions of the same protocol to reduce the noise of data. The best data among three were taken. Before taking any data, each subject will perform a short warm up. After that, each subject performed maximal voluntary isometric contraction task on a chair which were used to normalize other data (Figure 6.2). For vastus lateralis, vastus medialis and rectus femoris the leg will be extended to 45-degree and a person gave opposite force on the leg to get the maximum contraction (Simenz, Garceau, Lutsch, Suchomel, & Ebben, 2012). Bicep femoris was measure at 60-degree knee flexion and a

person will similarly oppose his leg to get maximum contraction of the muscle (Simenz et al., 2012).

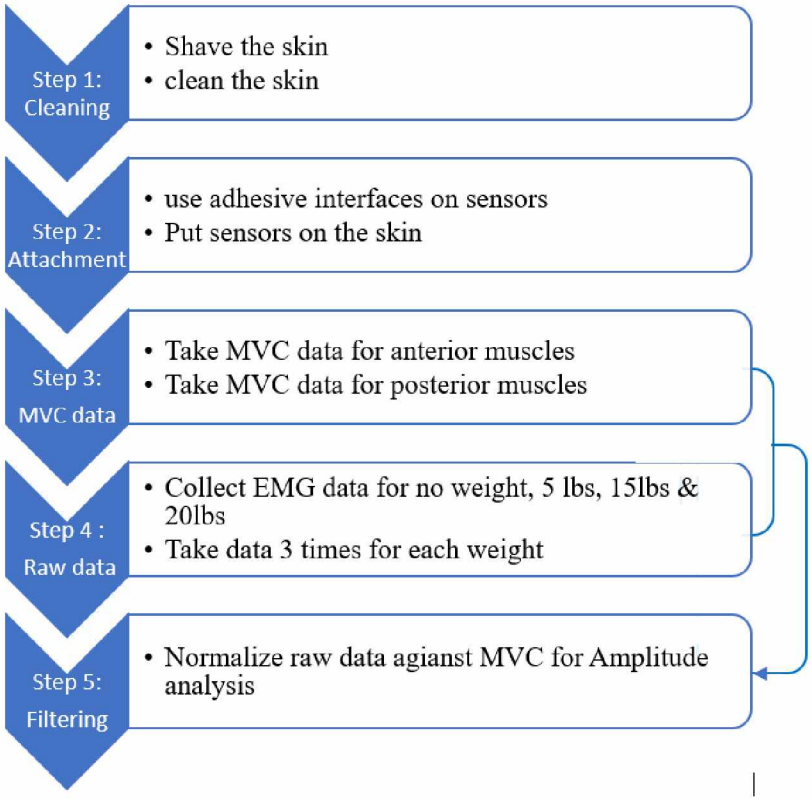

Figure 6. 4 Flow diagram of EMG data collection and filtering

Step 4 (Raw data): Subjects repetitively lift a weight from floor to a chest level height like the simulation in OpenSim. The weights were varied from no load, 5 lbs., 15 lbs. and 20 lbs. After each complete lift, the subject took 20 second rest.

Step 5 (Filtering): Comparing each muscle's data with the maximum voluntary contraction of that muscle gives us the percentage of muscle utilization. This is called amplitude analysis. At first, a root mean square (RMS) is performed on the input raw data. For this, we took the RMS window length 0.125 second and RMS window overlap 0.0625 second. The longer the window length, the system will take more value to calculate each RMS. As a result, more averaging will take place

and it will be less responsive but more accurate. After that, it normalizes the RMS data against another series which were taken at Step 3. Normalization helps to compare various kinds of data range at a same platform from 0 to 1.

6.4 Data acquisition

Data are collected from six EMG sensors from leg muscles (Figure 6.5). The range of raw data is from micro volts to millivolts.

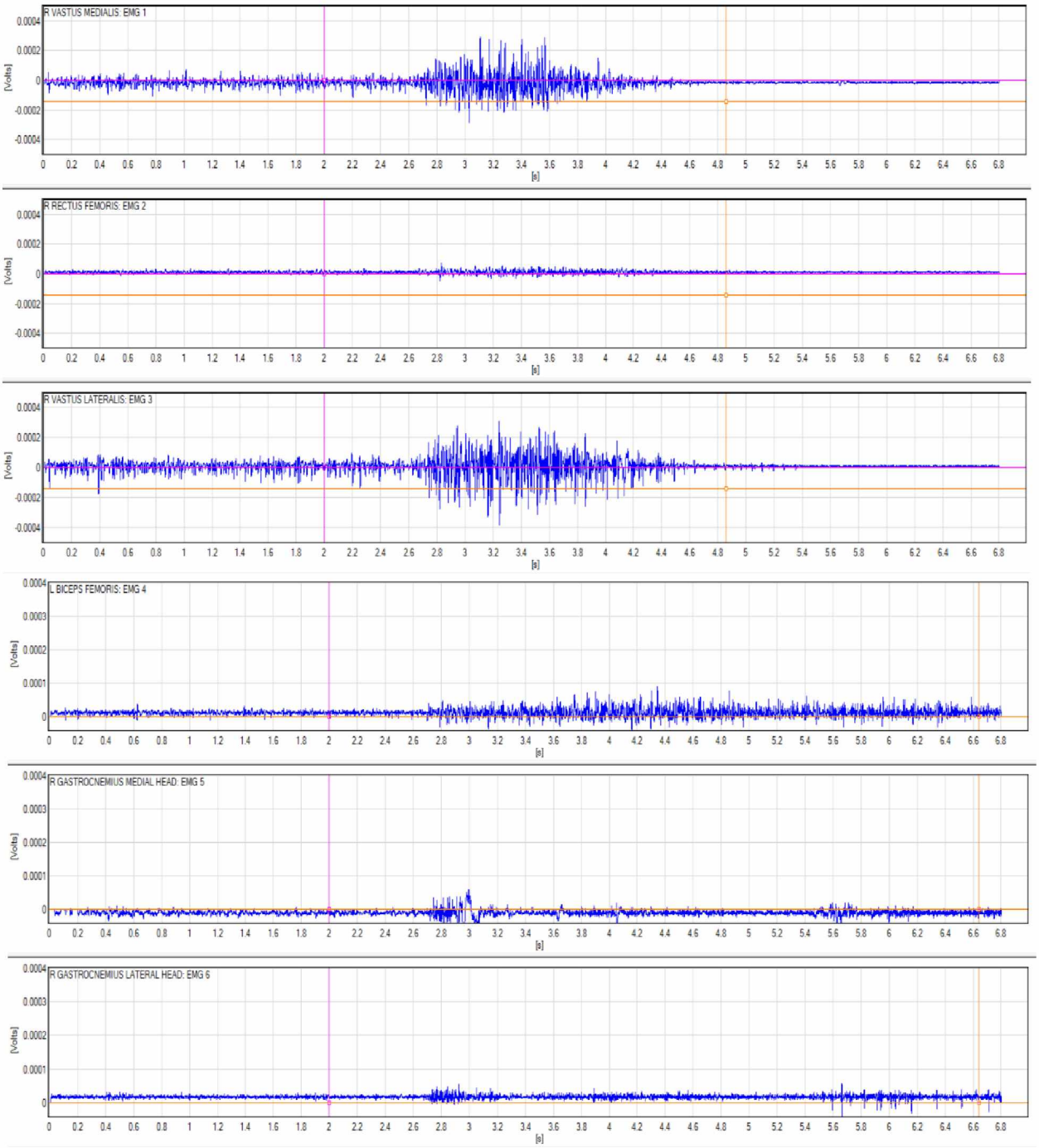

Figure 6. 5 Raw EMG data

6.5 Results and conclusion

During the course of lifting, activity of quadriceps muscles i.e. vastus medialis, rectus femoris and vastus laterals increased as the subject started to lift. These muscles are from anterior

side of thigh. Muscle activity of posterior side i.e. bicep femoris, gastrocnemius medial and lateral head increased just before the time of standing straight. Amplitude of the EMG signal spike increased as the lifted load increased.

From the filtered data in Figure 6.6, it can be seen that quadriceps muscles, in particular the vastus medialis and vastus lateralis muscle groups, are highly activated. For a couple of seconds, vastus medialis and vastus lateralis are activated about 80% and 45%, respectively. This means these two muscles are over-utilizing for a limited time. Muscles can be activated more than 100% for only few seconds. If these two muscles are utilized over 100% for long time, there is a high chance to be harmed. Gastrocnemius medial head and gastrocnemius lateral head muscles are also activated for about 40% and 30%, respectively. However, these two lower leg muscles were activated later to balance the body at the standing position.

The output of OpenSim and EMG data are quite similar. From the OpenSim simulations, we also found out that the muscle fiber forces from vastus lateralis and vastus medialis were high. Although we instructed the subject to use the strategy of max weightlifting for a regular weight, the distance and height also have a significant effect on lifting. That's why although we found similar results, we cannot compare them directly in this case.

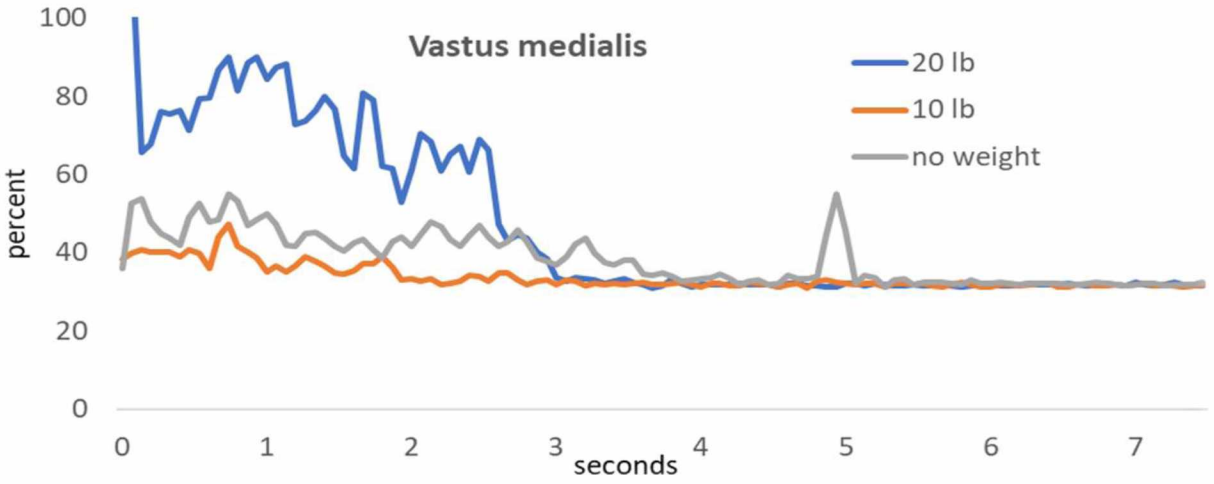
Vastus medialis
20 lb
10 lb
no weight
percent
100
80
60
40
20
0
0
1
2
3
4
5
6
7
seconds

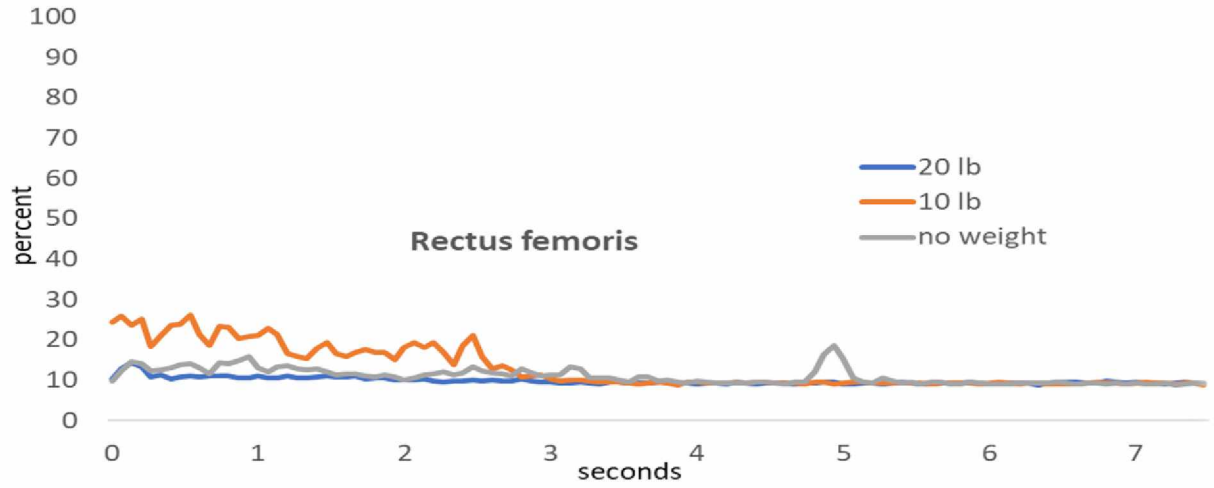
Rectus femoris
20 lb
10 lb
no weight
percent
100
90
80
70
60
50
40
30
20
10
0
0
1
2
3
4
5
6
7
seconds

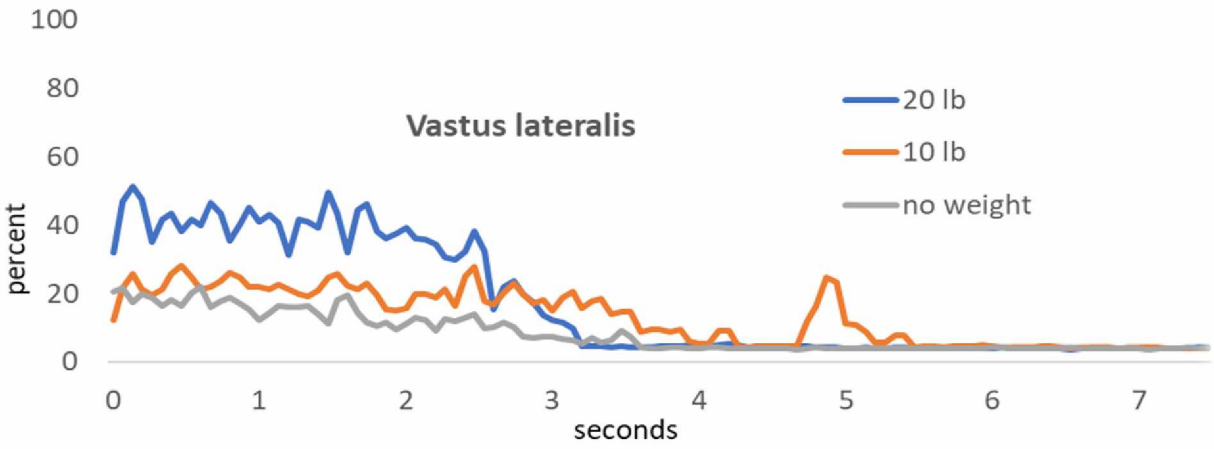
Vastus lateralis
20 lb
10 lb
no weight
percent
100
80
60
40
20
0
0
1
2
3
4
5
6
7
seconds

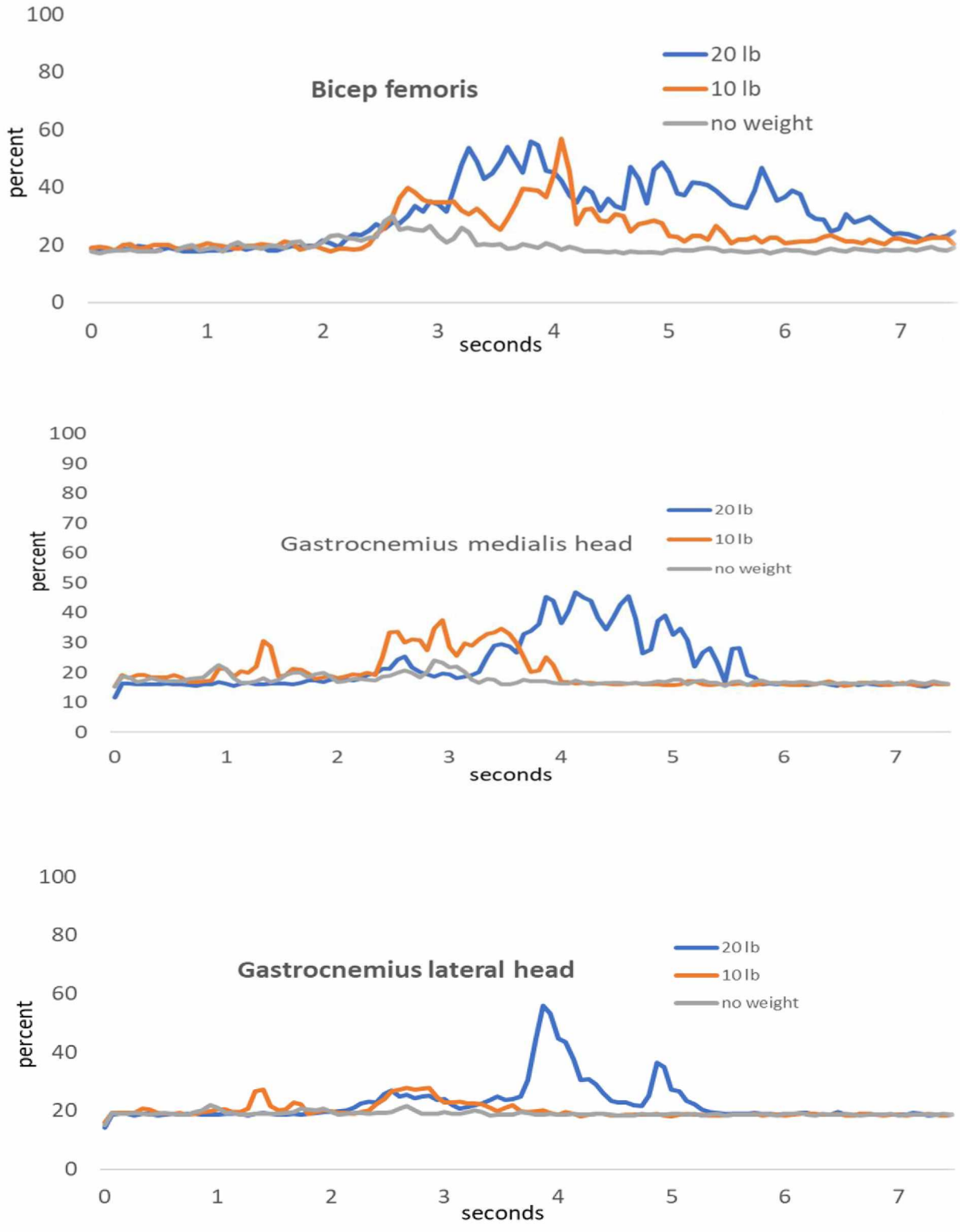

Figure 6. 6 Amplitude analysis of right leg muscle comparison for no load (red line), 10 lb (blue line) and 20 lb (green line)

Currently, the analysis of EMG data is very helpful for medical and biomechanics investigation. Biofeedback applications like training of specific muscles or ergonomic assessments are widely dependent on EMG data, although the relationship between force and surface EMG is not yet well understood (Delsys, 2018). Some authors proved that for various muscles EMG signals are directly proportional to muscle strength for isometric or isotonic contractions with constant speed, but other authors claimed that the relationship is non-linear (Kuriki et al., 2012). Some authors concluded that for isometric contraction, if the motor units independently activated, the amplitude of the signal is proportional to the square root of the force generated (Kuriki et al., 2012). The EMG signal from a sensor is a composite signal from all the muscles underlying the skin. Factors that prevent to conclude to a decision about the relation between electromyography data and muscle force are cross-talk between muscles, variations of the placement of electrodes on muscle belly and the difference between the motion generated by the subject during experiments.

Although there are arguments about the exact relation between the EMG data and force, there is a qualitative relationship between them (Delsys, 2018) . That's why EMG analysis is widely used for variety of clinical and biomedical applications, i.e. identifying the neuromuscular disorder, studying the tool for kinesiology, or controlling the signal for prosthetic devices.

Chapter 7 Conclusion and Future Work

7.1 Conclusion

In this thesis, an efficient optimization method is developed to predict the maximum lifting weight considering dynamic joint strength. Dynamic joint strength is modeled as a three-dimensional function of joint angle and velocity based on experimental data. In this prediction, the Denavit-Hartenberg (DH) method is used to express the kinematics of mechanics joints. The logistic equations are used to model the peak torque as a function of both joint angle and angular velocity, and the coefficients of the logistic function are obtained from Gauss least square regressions. The optimization problem is formulated as a nonlinear programming (NLP) using cubic B-spline discretization. Also, the dynamic joint strengths are considered as constraints which help us to predict the maximum lifting weight. In the proposed optimization, the external load is treated as design variables. By using this new formulation, dynamic lifting motion and strategy can be predicted for a symmetric maximum weight box lifting task with given initial and final box locations. The prediction outputs in joint space are integrated with OpenSim software to analyze muscle force and activity. Computed muscle control (CMC) is used to analyze muscle activity in OpenSim. We transferred joint angles, center of pressure and ground reaction forces from our predictive model to OpenSim. Using OpenSim, we can not only obtain muscle forces, but also decide which muscles need to be focused and analyzed for a particular motion. After that, we used EMG sensors to analyze leg muscles for a regular weight box lifting. We found some similarities between OpenSim simulations and EMG experiments, such as that Vastus muscles are highly activated. We were unable to compare these two directly, as our predictive and OpenSim models are for maximum weight, whereas EMG data were collected for a regular 20 lb weight. We can predict lifting strategy and maximum lifting weight using our predictive model. On the other hand,

using OpenSim and EMG data we can analyze muscle activity to find out sensitive muscles for lifting weight.

7.2 Future Work

1. The proposed predictive model is joint strength-based skeleton simulation. The muscle strength and activities are not calculated in this model. A predictive model based on both joint angles and muscle excitation-contraction dynamics will be more accurate and realistic. For this purpose, a 3D musculoskeletal model for dynamic lifting prediction with dynamic joint strength will be developed.

2. The EMG data collected in this research will be compared to the OpenSim simulation data directly. To do that, a subject's lifting motion using our predictive model will be simulated. Then transfer the predictive simulation results into OpenSim to obtain muscle activity information. Finally, these muscle activities from OpenSim will be compared to the EMG data. Therefore, it can validate our analysis loop of the predictive model, OpenSim, and the experimental EMG. The goal is to develop a robust simulation and analysis tool for lifting. This tool can also predict the lifting motion and muscle forces consider dynamic joint strength.

Reference

Aberg, U., Elgstrand, K., Magnus, P., & Lindholm, A. (1967). Analysts of components and prediction of energy expenditure in manual tasks. *The International Journal of Production Research, 6*(3), 189-196.

Ackermann, M., & Van den Bogert, A. J. (2010). Optimality principles for model-based prediction of human gait. *Journal of Biomechanics, 43*(6), 1055-1060.

Anderson, F. C., & Pandy, M. G. (2001). Dynamic optimization of human walking. *J Biomech Eng, 123*(5), 381-390.

Arisumi, H., Chardonnet, J.-R., Kheddar, A., & Yokoi, K. (2007). *Dynamic lifting motion of humanoid robots.* Paper presented at the Robotics and Automation, 2007 IEEE International Conference on.

Arnold, E. M., & Delp, S. L. (2011). Fibre operating lengths of human lower limb muscles during walking. *Philos Trans R Soc Lond B Biol Sci, 366*(1570), 1530-1539. doi:10.1098/rstb.2010.0345

Arora, J., & Wang, Q. (2005). Review of formulations for structural and mechanical system optimization. *Structural and Multidisciplinary Optimization, 30*(4), 251-272.

Asfour, S. S. (1980). *Energy cost prediction models for manual lifting and lowering tasks.* Texas Tech University,

Ayoub, M. (1992). Problems and solutions in manual materials handling: the state of the art. *Ergonomics, 35*(7-8), 713-728.

Ayoub, M., & Dempsey, P. G. (1999). The psychophysical approach to manual materials handling task design. *Ergonomics, 42*(1), 17-31.

Ayoub, M. M. (1989). *Manual materials handling: Design and injury control through ergonomics*: CRC Press.

Bermosa, N. (2010, Mar 8, 2018). The Strongest Muscles and the Largest Human Body Parts. Retrieved from https://physiology.knoji.com/the-strongest-muscles-and-the-largest-human-body-parts-2/

Burgess-Limerick, R., & Abernethy, B. (1997a). Toward a quantitative definition of manual lifting postures. *Human factors, 39*(1), 141-148.

Burgess-Limerick, R., & Abernethy, B. (1997b). Toward a Quantitative Definition of Manual Lifting Postures. *Human Factors: The Journal of the Human Factors and Ergonomics Society, 39*(1), 141-148. doi:10.1518/001872097778940632

Cahalan, T., Johnson, M., Liu, S., & Chao, E. Y. (1989). Quantitative measurements of hip strength in different age groups. *Clinical Orthopaedics and Related Research*(246), 136-145.

Ciriello, V., Snook, S., Buck, A., & Wilkinson, P. (1990). The effects of task duration on psychophysically-determined maximum acceptable weights and forces. *Ergonomics, 33*(2), 187-200.

Ciriello, V. M., Snook, S. H., Buck, A. C., & Wilkinson, P. L. (1990). The effects of task duration on psychophysically-determined maximum acceptable weights and forces. *Ergonomics, 33*(2), 187-200. doi:10.1080/00140139008927109

Davoudabadi Farahani, S., Andersen, M. S., de Zee, M., & Rasmussen, J. (2015). Optimization-based dynamic prediction of kinematic and kinetic patterns for a human vertical jump from a squatting position. *Multibody System Dynamics, 36*(1), 37-65. doi:10.1007/s11044-015-9468-5

Delsys. (2018). Technical Note 103 : EMG signal analysis. Retrieved from http://delsys.com/Attachments_pdf/download/technical-notes/103_emg-signal-analysis.pdf

Denavit, J. H., Richard Scheunemann. (1955). A kinematic notation for lower-pair mechanisms based on matrices. *Trans ASME J. Appl. Mech. 23: 215–221.*

Dooley, K. (2018). Anatomy Angel: Short Head, Biceps Femoris. Retrieved from http://www.drdooleynoted.com/anatomy-angel-short-head-biceps-femoris/

Dysart, M. J., & Woldstad, J. C. (1996). Posture prediction for static sagittal-plane lifting. *Journal of Biomechanics, 29*(10), 1393-1397.

Eisenberg, E., Hill, T. L., & Chen, Y. (1980). Cross-bridge model of muscle contraction. Quantitative analysis. *Biophys J, 29*(2), 195-227. doi:10.1016/S0006-3495(80)85126-5

Ekstrom, R. A., Donatelli, R. A., & Carp, K. C. (2007). Electromyographic analysis of core trunk, hip, and thigh muscles during 9 rehabilitation exercises. *journal of orthopaedic & sports physical therapy, 37*(12), 754-762.

Farahani, S. D., Andersen, M. S., de Zee, M., & Rasmussen, J. (2016). Optimization-based dynamic prediction of kinematic and kinetic patterns for a human vertical jump from a squatting position. *Multibody System Dynamics, 36*(1), 37-65.

Farizeh, T., & Sadigh, M. J. (2017). A mathematical framework to study fast walking of human. *Multibody System Dynamics, 40*(2), 99-122.

Frederik, W. (1959). Human energy in manual lifting. *Modern Materials Handling, 14*(3), 74-76.

Fregly, B. J., Reinbolt, J. A., Rooney, K. L., Mitchell, K. H., & Chmielewski, T. L. (2007). Design of patient-specific gait modifications for knee osteoarthritis rehabilitation. *IEEE Transactions on Biomedical Engineering, 54*(9), 1687-1695.

Freivalds, A., Chaffin, D. B., Garg, A., & Lee, K. S. (1984). A dynamic biomechanical evaluation of lifting maximum acceptable loads. *Journal of Biomechanics, 17*(4), 251-262.

Frey-Law, L. A., Laake, A., Avin, K. G., Heitsman, J., Marler, T., & Abdel-Malek, K. (2012). Knee and elbow 3D strength surfaces: peak torque-angle-velocity relationships. *Journal of Applied Biomechanics, 28*(6), 726-737.

Gill, P. E., Murray, W., & Saunders, M. A. (2002). SNOPT: An SQP Algorithm for Large-Scale Constrained Optimization. *SIAM Journal on Optimization, 12*(4), 979-1006. doi:10.1137/s1052623499350013

Haselgrove, J. C., & Huxley, H. E. (1973). X-ray evidence for radial cross-bridge movement and for the sliding filament model in actively contracting skeletal muscle. *J Mol Biol, 77*(4), 549-568.

Hill, A. V. (1949). The heat of activation and the heat of shortening in a muscle twitch. *Proc R Soc Lond B Biol Sci, 136*(883), 195-211.

Hollerbach, J. M. (1980). A Recursive Lagrangian Formulation of Maniputator Dynamics and a Comparative Study of Dynamics Formulation Complexity. *IEEE Transactions on Systems, Man, and Cybernetics, 10*(11), 730-736. doi:10.1109/tsmc.1980.4308393

Huang, C., Sheth, P. N., & Granata, K. P. (2005). *Multibody dynamics integrated with muscle models and space-time constraints for optimization of lifting movements.* Paper presented at the ASME 2005 International Design Engineering Technical Conferences and Computers and Information in Engineering Conference.

Hussain, S. J., & Frey-Law, L. (2016). 3D strength surfaces for ankle plantar- and dorsi-flexion in healthy adults: an isometric and isokinetic dynamometry study. *Journal of Foot and Ankle Research, 9*(1). doi:10.1186/s13047-016-0174-1

Hussain, S. J., & Frey-Law, L. (2016). 3D strength surfaces for ankle plantar-and dorsi-flexion in healthy adults: an isometric and isokinetic dynamometry study. *Journal of Foot and Ankle Research, 9*(1), 43.

Jakobsen, M. D., Sundstrup, E., Andersen, C. H., Aagaard, P., & Andersen, L. L. (2013). Muscle activity during leg strengthening exercise using free weights and elastic resistance: effects of ballistic vs controlled contractions. *Hum Mov Sci, 32*(1), 65-78. doi:10.1016/j.humov.2012.07.002

Knipfer, R. E. (1974). *Predictive models for the maximum acceptable weight of lift.* Texas Tech University,

Kothiyał, K., Mazumdar, J., & Noone, G. (1992). A biomechanical model for optimal postures in manual lifting tasks. *International Journal of Industrial Ergonomics, 10*(3), 241-255.

Kumar, S. (1996). Isolated planar trunk strengths measurement in normals: Part iii—results and database. *International Journal of Industrial Ergonomics, 17*(2), 103-111.

Kuriki, H. U., De Azevedo, F. M., Takahashi, L. S. O., Mello, E. M., de Faria Negrão Filho, R., & Alves, N. (2012). The relationship between electromyography and muscle force. In *EMG Methods for evaluating muscle and nerve function*: InTech.

Lee, Y. (1988). *An optimization model to evaluate methods of manual lifting.* Ph. D. thesis, Department of Industrial Engineering, Texas Tech University,

Looft, J. M. (2014). *Adaptation and validation of an analytical localized muscle fatigue model for workplace tasks*: The University of Iowa.

Marcelo Epstein , W. H. (1998). *Theoretical Models of Skeletal Muscle: Biological and Mathematical Considerations*.

McConville, J. T. H., H.T.E. (1992). *A study of one handed lifting: final report.* Retrieved from

Millard, M., Uchida, T., Seth, A., & Delp, S. L. (2013). Flexing computational muscle: modeling and simulation of musculotendon dynamics. *J Biomech Eng, 135*(2), 021005. doi:10.1115/1.4023390

Millard, M., Uchida, T., Seth, A., & Delp, S. L. (2013). Flexing Computational Muscle: Modeling and Simulation of Musculotendon Dynamics. *Journal of Biomechanical Engineering, 135*(2), 021005. doi:10.1115/1.4023390

Muscle Contraction and Locomotion. Retrieved from https://courses.lumenlearning.com/boundless-biology/chapter/muscle-contraction-and-locomotion/

Noone, G., & Mazumdar, J. (1992). Lifting low-lying loads in the sagittal plane. *Ergonomics, 35*(1), 65-92.

Osgood, R. T. (1980). *An investigation of the maximum acceptable weight of lift for bags.* Georgia Institute of Technology,

Pinder, A., & Boocock, M. (2014). Prediction of the maximum acceptable weight of lift from the frequency of lift. *International Journal of Industrial Ergonomics, 44*(2), 225-237.

Pinder, A. D. J. (1997). *Literature review: the relationship between load and frequency in manual handling operations*. Retrieved from

Pinder, A. D. J., & Boocock, M. G. (2014). Prediction of the maximum acceptable weight of lift from the frequency of lift. *International Journal of Industrial Ergonomics, 44*(2), 225-237. doi:10.1016/j.ergon.2012.11.005

Pytel, J. L., & Kamon, E. (1981). Dynamic strength test as a predictor for maximal and acceptable lifting. *Ergonomics, 24*(9), 663-672.
Ren, L., Jones, R. K., & Howard, D. (2007). Predictive modelling of human walking over a complete gait cycle. *Journal of Biomechanics, 40*(7), 1567-1574.
Selbie, W. S., & Caldwell, G. E. (1996). A simulation study of vertical jumping from different starting postures. *Journal of Biomechanics, 29*(9), 1137-1146. doi:https://doi.org/10.1016/0021-9290(96)00030-9
Shourijeh, M. S., & McPhee, J. (2014). Forward dynamic optimization of human gait simulations: a global parameterization approach. *Journal of Computational and Nonlinear Dynamics, 9*(3), 031018.
Simenz, C. J., Garceau, L. R., Lutsch, B. N., Suchomel, T. J., & Ebben, W. P. (2012). Electromyographical analysis of lower extremity muscle activation during variations of the loaded step-up exercise. *The Journal of Strength & Conditioning Research, 26*(12), 3398-3405.
Snook, S. H., & Ciriello, V. M. (1974). Maximum weights and work loads acceptable to female workers. *Journal of Occupational and Environmental Medicine, 16*(8), 527-534.
Song, J., Qu, X., & Chen, C.-H. (2016). Simulation of lifting motions using a novel multi-objective optimization approach. *International Journal of Industrial Ergonomics, 53*, 37-47.
Stockdale, A. A. (2011). *Modeling three-dimensional hip and trunk peak torque as a function of joint angle and velocity*: The University of Iowa.
Stovall, G. (2013, November 26, 2013). Breakdown Of Skeletal Muscle Tissue. Retrieved from http://pulpbits.net/3-breakdown-of-skeletal-muscle-tissue/breakdown-of-skeletal-muscle-tissue/
Switzer, S. (1962). *Weight-lifting capabilities of a selected sample of human males*. Retrieved from
Thelen, D. G. (2003). Adjustment of muscle mechanics model parameters to simulate dynamic contractions in older adults. *J Biomech Eng, 125*(1), 70-77.
Thelen, D. G., & Anderson, F. C. (2006). Using computed muscle control to generate forward dynamic simulations of human walking from experimental data. *J Biomech, 39*(6), 1107-1115. doi:10.1016/j.jbiomech.2005.02.010
Thelen, D. G., & Anderson, F. C. (2006). Using computed muscle control to generate forward dynamic simulations of human walking from experimental data. *Journal of Biomechanics, 39*(6), 1107-1115.
Thelen, D. G., Anderson, F. C., & Delp, S. L. (2003). Generating dynamic simulations of movement using computed muscle control. *J Biomech, 36*(3), 321-328.
Toogood, R. W. (1989). *Efficient robot inverse and direct dynamics algorithms using microcomputer based symbolic generation*. Paper presented at the Proceedings, 1989 International Conference on Robotics and Automation. http://dx.doi.org/10.1109/robot.1989.100239
TRIGNO Wireless System User's Guide. (2014). Retrieved from www.delsys.com
Van der Krogt, M. M., Delp, S. L., & Schwartz, M. H. (2012). How robust is human gait to muscle weakness? *Gait & Posture, 36*(1), 113-119. doi:https://doi.org/10.1016/j.gaitpost.2012.01.017

Willms, E. (2012). How Does a Muscle Contract ERW. Retrieved from http://humanbiologylab.pbworks.com/w/page/60188315/How%20Does%20a%20Muscle%20Contract%20ERW

Winters, J. M., & Stark, L. (1987). Muscle models: what is gained and what is lost by varying model complexity. *Biol Cybern, 55*(6), 403-420.

Xiang, Y., Arora, J. S., & Abdel-Malek, K. (2008). Optimization-based motion prediction of mechanical systems: sensitivity analysis. *Structural and Multidisciplinary Optimization, 37*(6), 595-608. doi:10.1007/s00158-008-0247-2

Xiang, Y., Arora, J. S., & Abdel-Malek, K. (2010). Physics-based modeling and simulation of human walking: a review of optimization-based and other approaches. *Structural and Multidisciplinary Optimization, 42*(1), 1-23.

Xiang, Y., Arora, J. S., & Abdel-Malek, K. (2012). 3D HUMAN LIFTING MOTION PREDICTION WITH DIFFERENT PERFORMANCE MEASURES. *International Journal of Humanoid Robotics, 09*(02), 1250012. doi:10.1142/s0219843612500120

Xiang, Y., Arora, J. S., & Abdel-Malek, K. (2012). 3D human lifting motion prediction with different performance measures. *International Journal of Humanoid Robotics, 9*(02), 1250012.

Xiang, Y., Arora, J. S., Rahmatalla, S., & Abdel-Malek, K. (2009). Optimization-based dynamic human walking prediction: One step formulation. *International Journal for Numerical Methods in Engineering, 79*(6), 667-695. doi:10.1002/nme.2575

Xiang, Y., Arora, J. S., Rahmatalla, S., & Abdel-Malek, K. (2009). Optimization-based dynamic human walking prediction: One step formulation. *International Journal for Numerical Methods in Engineering, 79*(6), 667-695.

Xiang, Y., Arora, J. S., Rahmatalla, S., Marler, T., Bhatt, R., & Abdel-Malek, K. (2010). Human lifting simulation using a multi-objective optimization approach. *Multibody System Dynamics, 23*(4), 431-451. doi:10.1007/s11044-009-9186-y

Zahalak, G. I., & Ma, S. P. (1990). Muscle activation and contraction: constitutive relations based directly on cross-bridge kinetics. *J Biomech Eng, 112*(1), 52-62.

Zajac, F. E. (1989). Muscle and tendon: properties, models, scaling, and application to biomechanics and motor control. *Crit Rev Biomed Eng, 17*(4), 359-411.

Zajac, F. E., Neptune, R. R., & Kautz, S. A. (2002). Biomechanics and muscle coordination of human walking. Part I: introduction to concepts, power transfer, dynamics and simulations. *Gait Posture, 16*(3), 215-232.

Zajac, F. E., Neptune, R. R., & Kautz, S. A. (2003). Biomechanics and muscle coordination of human walking: part II: lessons from dynamical simulations and clinical implications. *Gait Posture, 17*(1), 1-17.

Zhang, X., Nussbaum, M. A., & Chaffin, D. B. (2000). Back lift versus leg lift: an index and visualization of dynamic lifting strategies. *Journal of Biomechanics, 33*(6), 777-782.

Appendix

Table A 1. Joint angle limits

Joint name	Lower limit	Upper limit
Global translation 1 (forward) (m)	-5.0	5.0
Global translation 2 (upward) (m)	-5.0	5.0
Global rotation (deg)	0.0	0.0
Spine (deg)	0.0	90.0
Shoulder (deg)	-180.0	90.0
Elbow (deg)	-150.0	0.0
Hip (deg)	-100.0	90.0
Knee (deg)	0.0	120.0
Ankle (deg)	-20.0	80.0
Metatarsal (deg)	-60.0	0.0

Table A 2. Static joint torque limits (N·m)

Joint name	Lower limit	Upper limit
Global translation 1 (forward)	-500.0	500.0
Global translation 2 (upward)	-500.0	500.0
Global rotation	-500.0	500.0
Spine	-400.0	400.0
Shoulder	-184.0	126.0
Elbow	-117.4	120.6
Hip	-334.0	408.0
Knee	-518.2	206.4
Ankle	-75.4	170.6
Metatarsal	-140.0	140.0

Note that the arm and leg strength are doubled because arms and legs are modeled as single branches.